

1 **Measurement of CP-violating asymmetries in  $D^0 \rightarrow \pi^+\pi^-$  and**  
2  **$D^0 \rightarrow K^+K^-$  decays at CDF**

3 T. Aaltonen,<sup>21</sup> B. Álvarez González<sup>z</sup>,<sup>9</sup> S. Amerio,<sup>40</sup> D. Amidei,<sup>32</sup> A. Anastassov<sup>x</sup>,<sup>15</sup>  
4 A. Annovi,<sup>17</sup> J. Antos,<sup>12</sup> G. Apollinari,<sup>15</sup> J.A. Appel,<sup>15</sup> T. Arisawa,<sup>54</sup> A. Artikov,<sup>13</sup>  
5 J. Asaadi,<sup>49</sup> W. Ashmanskas,<sup>15</sup> B. Auerbach,<sup>57</sup> A. Aurisano,<sup>49</sup> F. Azfar,<sup>39</sup> W. Badgett,<sup>15</sup>  
6 T. Bae,<sup>25</sup> A. Barbaro-Galtieri,<sup>26</sup> V.E. Barnes,<sup>44</sup> B.A. Barnett,<sup>23</sup> P. Barria<sup>hh</sup>,<sup>42</sup>  
7 P. Bartos,<sup>12</sup> M. Bauce<sup>ff</sup>,<sup>40</sup> F. Bedeschi,<sup>42</sup> S. Behari,<sup>23</sup> G. Bellettini<sup>gg</sup>,<sup>42</sup> J. Bellinger,<sup>56</sup>  
8 D. Benjamin,<sup>14</sup> A. Beretvas,<sup>15</sup> A. Bhatti,<sup>46</sup> D. Bisello<sup>ff</sup>,<sup>40</sup> I. Bizjak,<sup>28</sup> K.R. Bland,<sup>5</sup>  
9 B. Blumenfeld,<sup>23</sup> A. Bocci,<sup>14</sup> A. Bodek,<sup>45</sup> D. Bortoletto,<sup>44</sup> J. Boudreau,<sup>43</sup> A. Boveia,<sup>11</sup>  
10 L. Brigliadori<sup>ee</sup>,<sup>6</sup> C. Bromberg,<sup>33</sup> E. Brucken,<sup>21</sup> J. Budagov,<sup>13</sup> H.S. Budd,<sup>45</sup> K. Burkett,<sup>15</sup>  
11 G. Busetto<sup>ff</sup>,<sup>40</sup> P. Bussey,<sup>19</sup> A. Buzatu,<sup>31</sup> A. Calamba,<sup>10</sup> C. Calancha,<sup>29</sup> S. Camarda,<sup>4</sup>  
12 M. Campanelli,<sup>28</sup> M. Campbell,<sup>32</sup> F. Canelli<sup>11</sup>,<sup>15</sup> B. Carls,<sup>22</sup> D. Carlsmith,<sup>56</sup>  
13 R. Carosi,<sup>42</sup> S. Carrillo<sup>m</sup>,<sup>16</sup> S. Carron,<sup>15</sup> B. Casal<sup>k</sup>,<sup>9</sup> M. Casarsa,<sup>50</sup> A. Castro<sup>ee</sup>,<sup>6</sup>  
14 P. Catastini,<sup>20</sup> D. Cauz,<sup>50</sup> V. Cavaliere,<sup>22</sup> M. Cavalli-Sforza,<sup>4</sup> A. Cerri<sup>f</sup>,<sup>26</sup> L. Cerrito<sup>s</sup>,<sup>28</sup>  
15 Y.C. Chen,<sup>1</sup> M. Chertok,<sup>7</sup> G. Chiarelli,<sup>42</sup> G. Chlachidze,<sup>15</sup> F. Chlebana,<sup>15</sup> K. Cho,<sup>25</sup>  
16 D. Chokheli,<sup>13</sup> W.H. Chung,<sup>56</sup> Y.S. Chung,<sup>45</sup> M.A. Ciocci<sup>hh</sup>,<sup>42</sup> A. Clark,<sup>18</sup> C. Clarke,<sup>55</sup>  
17 G. Compostella<sup>ff</sup>,<sup>40</sup> M.E. Convery,<sup>15</sup> J. Conway,<sup>7</sup> M. Corbo,<sup>15</sup> M. Cordelli,<sup>17</sup> C.A. Cox,<sup>7</sup>  
18 D.J. Cox,<sup>7</sup> F. Crescioli<sup>gg</sup>,<sup>42</sup> J. Cuevas<sup>z</sup>,<sup>9</sup> R. Culbertson,<sup>15</sup> D. Dagenhart,<sup>15</sup> N. d'Ascenzo<sup>w</sup>,<sup>15</sup>  
19 M. Datta,<sup>15</sup> P. de Barbaro,<sup>45</sup> M. Dell'Orso<sup>gg</sup>,<sup>42</sup> L. Demortier,<sup>46</sup> M. Deninno,<sup>6</sup> F. Devoto,<sup>21</sup>  
20 M. d'Errico<sup>ff</sup>,<sup>40</sup> A. Di Canto<sup>gg</sup>,<sup>42</sup> B. Di Ruzza,<sup>15</sup> J.R. Dittmann,<sup>5</sup> M. D'Onofrio,<sup>27</sup>  
21 S. Donati<sup>gg</sup>,<sup>42</sup> P. Dong,<sup>15</sup> M. Dorigo,<sup>50</sup> T. Dorigo,<sup>40</sup> K. Ebina,<sup>54</sup> A. Elagin,<sup>49</sup> A. Eppig,<sup>32</sup>  
22 R. Erbacher,<sup>7</sup> S. Errede,<sup>22</sup> N. Ershaidat<sup>dd</sup>,<sup>15</sup> R. Eusebi,<sup>49</sup> S. Farrington,<sup>39</sup> M. Feindt,<sup>24</sup>  
23 J.P. Fernandez,<sup>29</sup> R. Field,<sup>16</sup> G. Flanagan<sup>u</sup>,<sup>15</sup> R. Forrest,<sup>7</sup> M.J. Frank,<sup>5</sup> M. Franklin,<sup>20</sup>  
24 J.C. Freeman,<sup>15</sup> Y. Funakoshi,<sup>54</sup> I. Furic,<sup>16</sup> M. Gallinaro,<sup>46</sup> J.E. Garcia,<sup>18</sup> A.F. Garfinkel,<sup>44</sup>  
25 P. Garosi<sup>hh</sup>,<sup>42</sup> H. Gerberich,<sup>22</sup> E. Gerchtein,<sup>15</sup> S. Giagu,<sup>47</sup> V. Giakoumopoulou,<sup>3</sup>  
26 P. Giannetti,<sup>42</sup> K. Gibson,<sup>43</sup> C.M. Ginsburg,<sup>15</sup> N. Giokaris,<sup>3</sup> P. Giromini,<sup>17</sup> G. Giurgiu,<sup>23</sup>  
27 V. Glagolev,<sup>13</sup> D. Glenzinski,<sup>15</sup> M. Gold,<sup>35</sup> D. Goldin,<sup>49</sup> N. Goldschmidt,<sup>16</sup> A. Golossanov,<sup>15</sup>  
28 G. Gomez,<sup>9</sup> G. Gomez-Ceballos,<sup>30</sup> M. Goncharov,<sup>30</sup> O. González,<sup>29</sup> I. Gorelov,<sup>35</sup>  
29 A.T. Goshaw,<sup>14</sup> K. Goulianos,<sup>46</sup> S. Grinstein,<sup>4</sup> C. Grosso-Pilcher,<sup>11</sup> R.C. Group<sup>53</sup>,<sup>15</sup>

30 J. Guimaraes da Costa,<sup>20</sup> S.R. Hahn,<sup>15</sup> E. Halkiadakis,<sup>48</sup> A. Hamaguchi,<sup>38</sup> J.Y. Han,<sup>45</sup>  
 31 F. Happacher,<sup>17</sup> K. Hara,<sup>51</sup> D. Hare,<sup>48</sup> M. Hare,<sup>52</sup> R.F. Harr,<sup>55</sup> K. Hatakeyama,<sup>5</sup>  
 32 C. Hays,<sup>39</sup> M. Heck,<sup>24</sup> J. Heinrich,<sup>41</sup> M. Herndon,<sup>56</sup> S. Hewamanage,<sup>5</sup> A. Hocker,<sup>15</sup>  
 33 W. Hopkins<sup>g</sup>,<sup>15</sup> D. Horn,<sup>24</sup> S. Hou,<sup>1</sup> R.E. Hughes,<sup>36</sup> M. Hurwitz,<sup>11</sup> U. Husemann,<sup>57</sup>  
 34 N. Hussain,<sup>31</sup> M. Hussein,<sup>33</sup> J. Huston,<sup>33</sup> G. Introzzi,<sup>42</sup> M. Iori<sup>jj</sup>,<sup>47</sup> A. Ivanov<sup>p</sup>,<sup>7</sup> E. James,<sup>15</sup>  
 35 D. Jang,<sup>10</sup> B. Jayatilaka,<sup>14</sup> E.J. Jeon,<sup>25</sup> S. Jindariani,<sup>15</sup> M. Jones,<sup>44</sup> K.K. Joo,<sup>25</sup> S.Y. Jun,<sup>10</sup>  
 36 T.R. Junk,<sup>15</sup> T. Kamon<sup>25, 49</sup> P.E. Karchin,<sup>55</sup> A. Kasmi,<sup>5</sup> Y. Kato<sup>o</sup>,<sup>38</sup> W. Ketchum,<sup>11</sup>  
 37 J. Keung,<sup>41</sup> V. Khotilovich,<sup>49</sup> B. Kilminster,<sup>15</sup> D.H. Kim,<sup>25</sup> H.S. Kim,<sup>25</sup> J.E. Kim,<sup>25</sup>  
 38 M.J. Kim,<sup>17</sup> S.B. Kim,<sup>25</sup> S.H. Kim,<sup>51</sup> Y.K. Kim,<sup>11</sup> Y.J. Kim,<sup>25</sup> N. Kimura,<sup>54</sup> M. Kirby,<sup>15</sup>  
 39 S. Klimenko,<sup>16</sup> K. Knoepfel,<sup>15</sup> K. Kondo<sup>a</sup>,<sup>54</sup> D.J. Kong,<sup>25</sup> J. Konigsberg,<sup>16</sup> A.V. Kotwal,<sup>14</sup>  
 40 M. Kreps,<sup>24</sup> J. Kroll,<sup>41</sup> D. Krop,<sup>11</sup> M. Kruse,<sup>14</sup> V. Krutelyov<sup>c</sup>,<sup>49</sup> T. Kuhr,<sup>24</sup> M. Kurata,<sup>51</sup>  
 41 S. Kwang,<sup>11</sup> A.T. Laasanen,<sup>44</sup> S. Lami,<sup>42</sup> S. Lammel,<sup>15</sup> M. Lancaster,<sup>28</sup> R.L. Lander,<sup>7</sup>  
 42 K. Lannon<sup>y</sup>,<sup>36</sup> A. Lath,<sup>48</sup> G. Latino<sup>hh</sup>,<sup>42</sup> T. LeCompte,<sup>2</sup> E. Lee,<sup>49</sup> H.S. Lee<sup>q</sup>,<sup>11</sup> J.S. Lee,<sup>25</sup>  
 43 S.W. Lee<sup>bb</sup>,<sup>49</sup> S. Leo<sup>gg</sup>,<sup>42</sup> S. Leone,<sup>42</sup> J.D. Lewis,<sup>15</sup> A. Limosani<sup>t</sup>,<sup>14</sup> C.-J. Lin,<sup>26</sup>  
 44 M. Lindgren,<sup>15</sup> E. Lipeles,<sup>41</sup> A. Lister,<sup>18</sup> D.O. Litvintsev,<sup>15</sup> C. Liu,<sup>43</sup> H. Liu,<sup>53</sup> Q. Liu,<sup>44</sup>  
 45 T. Liu,<sup>15</sup> S. Lockwitz,<sup>57</sup> A. Loginov,<sup>57</sup> D. Lucchesi<sup>ff</sup>,<sup>40</sup> J. Lueck,<sup>24</sup> P. Lujan,<sup>26</sup> P. Lukens,<sup>15</sup>  
 46 G. Lungu,<sup>46</sup> J. Lys,<sup>26</sup> R. Lysak<sup>e</sup>,<sup>12</sup> R. Madrak,<sup>15</sup> K. Maeshima,<sup>15</sup> P. Maestro<sup>hh</sup>,<sup>42</sup>  
 47 S. Malik,<sup>46</sup> G. Manca<sup>a</sup>,<sup>27</sup> A. Manousakis-Katsikakis,<sup>3</sup> F. Margaroli,<sup>47</sup> C. Marino,<sup>24</sup>  
 48 M. Martínez,<sup>4</sup> P. Mastrandrea,<sup>47</sup> K. Matera,<sup>22</sup> M.E. Mattson,<sup>55</sup> A. Mazzacane,<sup>15</sup>  
 49 P. Mazzanti,<sup>6</sup> K.S. McFarland,<sup>45</sup> P. McIntyre,<sup>49</sup> R. McNulty<sup>j</sup>,<sup>27</sup> A. Mehta,<sup>27</sup> P. Mehtala,<sup>21</sup>  
 50 C. Mesropian,<sup>46</sup> T. Miao,<sup>15</sup> D. Mietlicki,<sup>32</sup> A. Mitra,<sup>1</sup> H. Miyake,<sup>51</sup> S. Moed,<sup>15</sup> N. Moggi,<sup>6</sup>  
 51 M.N. Mondragon<sup>m</sup>,<sup>15</sup> C.S. Moon,<sup>25</sup> R. Moore,<sup>15</sup> M.J. Morello<sup>ii</sup>,<sup>42</sup> J. Morlock,<sup>24</sup>  
 52 P. Movilla Fernandez,<sup>15</sup> A. Mukherjee,<sup>15</sup> Th. Muller,<sup>24</sup> P. Murat,<sup>15</sup> M. Mussini<sup>ee</sup>,<sup>6</sup>  
 53 J. Nachtman<sup>n</sup>,<sup>15</sup> Y. Nagai,<sup>51</sup> J. Naganoma,<sup>54</sup> I. Nakano,<sup>37</sup> A. Napier,<sup>52</sup> J. Nett,<sup>49</sup> C. Neu,<sup>53</sup>  
 54 M.S. Neubauer,<sup>22</sup> J. Nielsen<sup>d</sup>,<sup>26</sup> L. Nodulman,<sup>2</sup> S.Y. Noh,<sup>25</sup> O. Norniella,<sup>22</sup> L. Oakes,<sup>39</sup>  
 55 S.H. Oh,<sup>14</sup> Y.D. Oh,<sup>25</sup> I. Oksuzian,<sup>53</sup> T. Okusawa,<sup>38</sup> R. Orava,<sup>21</sup> L. Ortolan,<sup>4</sup>  
 56 S. Pagan Griso<sup>ff</sup>,<sup>40</sup> C. Pagliarone,<sup>50</sup> E. Palencia<sup>f</sup>,<sup>9</sup> V. Papadimitriou,<sup>15</sup> A.A. Paramonov,<sup>2</sup>  
 57 J. Patrick,<sup>15</sup> G. Pauletta<sup>kk</sup>,<sup>50</sup> M. Paulini,<sup>10</sup> C. Paus,<sup>30</sup> D.E. Pellett,<sup>7</sup> A. Penzo,<sup>50</sup>  
 58 T.J. Phillips,<sup>14</sup> G. Piacentino,<sup>42</sup> E. Pianori,<sup>41</sup> J. Pilot,<sup>36</sup> K. Pitts,<sup>22</sup> C. Plager,<sup>8</sup>

---

<sup>a</sup> Deceased

59 L. Pondrom,<sup>56</sup> S. Poprocki<sup>g</sup>,<sup>15</sup> K. Potamianos,<sup>44</sup> F. Prokoshin<sup>cc</sup>,<sup>13</sup> A. Pranko,<sup>26</sup>  
 60 F. Ptohos<sup>h</sup>,<sup>17</sup> G. Punzi<sup>gg</sup>,<sup>42</sup> A. Rahaman,<sup>43</sup> V. Ramakrishnan,<sup>56</sup> N. Ranjan,<sup>44</sup> I. Redondo,<sup>29</sup>  
 61 P. Renton,<sup>39</sup> M. Rescigno,<sup>47</sup> T. Riddick,<sup>28</sup> F. Rimondi<sup>ee</sup>,<sup>6</sup> L. Ristori<sup>42,15</sup> A. Robson,<sup>19</sup>  
 62 T. Rodrigo,<sup>9</sup> T. Rodriguez,<sup>41</sup> E. Rogers,<sup>22</sup> S. Rolli<sup>i</sup>,<sup>52</sup> R. Roser,<sup>15</sup> F. Ruffini<sup>hh</sup>,<sup>42</sup> A. Ruiz,<sup>9</sup>  
 63 J. Russ,<sup>10</sup> V. Rusu,<sup>15</sup> A. Safonov,<sup>49</sup> W.K. Sakumoto,<sup>45</sup> Y. Sakurai,<sup>54</sup> L. Santi<sup>kk</sup>,<sup>50</sup>  
 64 K. Sato,<sup>51</sup> V. Saveliev<sup>w</sup>,<sup>15</sup> A. Savoy-Navarro<sup>aa</sup>,<sup>15</sup> P. Schlabach,<sup>15</sup> A. Schmidt,<sup>24</sup>  
 65 E.E. Schmidt,<sup>15</sup> T. Schwarz,<sup>15</sup> L. Scodellaro,<sup>9</sup> A. Scribano<sup>hh</sup>,<sup>42</sup> F. Scuri,<sup>42</sup> S. Seidel,<sup>35</sup>  
 66 Y. Seiya,<sup>38</sup> A. Semenov,<sup>13</sup> F. Sforza<sup>hh</sup>,<sup>42</sup> S.Z. Shalhout,<sup>7</sup> T. Shears,<sup>27</sup> P.F. Shepard,<sup>43</sup>  
 67 M. Shimojima<sup>v</sup>,<sup>51</sup> M. Shochet,<sup>11</sup> I. Shreyber-Tecker,<sup>34</sup> A. Simonenko,<sup>13</sup> P. Sinervo,<sup>31</sup>  
 68 K. Sliwa,<sup>52</sup> J.R. Smith,<sup>7</sup> F.D. Snider,<sup>15</sup> A. Soha,<sup>15</sup> V. Sorin,<sup>4</sup> H. Song,<sup>43</sup> P. Squillacioti<sup>hh</sup>,<sup>42</sup>  
 69 M. Stancari,<sup>15</sup> R. St. Denis,<sup>19</sup> B. Stelzer,<sup>31</sup> O. Stelzer-Chilton,<sup>31</sup> D. Stentz<sup>x</sup>,<sup>15</sup>  
 70 J. Strologas,<sup>35</sup> G.L. Strycker,<sup>32</sup> Y. Sudo,<sup>51</sup> A. Sukhanov,<sup>15</sup> I. Suslov,<sup>13</sup> K. Takemasa,<sup>51</sup>  
 71 Y. Takeuchi,<sup>51</sup> J. Tang,<sup>11</sup> M. Tecchio,<sup>32</sup> P.K. Teng,<sup>1</sup> J. Thom<sup>g</sup>,<sup>15</sup> J. Thome,<sup>10</sup>  
 72 G.A. Thompson,<sup>22</sup> E. Thomson,<sup>41</sup> D. Toback,<sup>49</sup> S. Tokar,<sup>12</sup> K. Tollefson,<sup>33</sup> T. Tomura,<sup>51</sup>  
 73 D. Tonelli,<sup>15</sup> S. Torre,<sup>17</sup> D. Torretta,<sup>15</sup> P. Totaro,<sup>40</sup> M. Trovato<sup>ii</sup>,<sup>42</sup> F. Ukegawa,<sup>51</sup>  
 74 S. Uozumi,<sup>25</sup> A. Varganov,<sup>32</sup> F. Vázquez<sup>m</sup>,<sup>16</sup> G. Velev,<sup>15</sup> C. Vellidis,<sup>15</sup> M. Vidal,<sup>44</sup> I. Vila,<sup>9</sup>  
 75 R. Vilar,<sup>9</sup> J. Vizán,<sup>9</sup> M. Vogel,<sup>35</sup> G. Volpi,<sup>17</sup> P. Wagner,<sup>41</sup> R.L. Wagner,<sup>15</sup> T. Wakisaka,<sup>38</sup>  
 76 R. Wallny,<sup>8</sup> S.M. Wang,<sup>1</sup> A. Warburton,<sup>31</sup> D. Waters,<sup>28</sup> W.C. Wester III,<sup>15</sup> D. Whiteson<sup>b</sup>,<sup>41</sup>  
 77 A.B. Wicklund,<sup>2</sup> E. Wicklund,<sup>15</sup> S. Wilbur,<sup>11</sup> F. Wick,<sup>24</sup> H.H. Williams,<sup>41</sup> J.S. Wilson,<sup>36</sup>  
 78 P. Wilson,<sup>15</sup> B.L. Winer,<sup>36</sup> P. Wittich<sup>g</sup>,<sup>15</sup> S. Wolbers,<sup>15</sup> H. Wolfe,<sup>36</sup> T. Wright,<sup>32</sup> X. Wu,<sup>18</sup>  
 79 Z. Wu,<sup>5</sup> K. Yamamoto,<sup>38</sup> D. Yamato,<sup>38</sup> T. Yang,<sup>15</sup> U.K. Yang<sup>r</sup>,<sup>11</sup> Y.C. Yang,<sup>25</sup>  
 80 W.-M. Yao,<sup>26</sup> G.P. Yeh,<sup>15</sup> K. Yi<sup>n</sup>,<sup>15</sup> J. Yoh,<sup>15</sup> K. Yorita,<sup>54</sup> T. Yoshida<sup>l</sup>,<sup>38</sup> G.B. Yu,<sup>14</sup>  
 81 I. Yu,<sup>25</sup> S.S. Yu,<sup>15</sup> J.C. Yun,<sup>15</sup> A. Zanetti,<sup>50</sup> Y. Zeng,<sup>14</sup> C. Zhou,<sup>14</sup> and S. Zucchelli<sup>ee6</sup>

82 (CDF Collaboration<sup>b</sup>)

<sup>b</sup> With visitors from <sup>a</sup>Istituto Nazionale di Fisica Nucleare, Sezione di Cagliari, 09042 Monserrato (Cagliari), Italy, <sup>b</sup>University of CA Irvine, Irvine, CA 92697, USA, <sup>c</sup>University of CA Santa Barbara, Santa Barbara, CA 93106, USA, <sup>d</sup>University of CA Santa Cruz, Santa Cruz, CA 95064, USA, <sup>e</sup>Institute of Physics, Academy of Sciences of the Czech Republic, Czech Republic, <sup>f</sup>CERN, CH-1211 Geneva, Switzerland, <sup>g</sup>Cornell University, Ithaca, NY 14853, USA, <sup>h</sup>University of Cyprus, Nicosia CY-1678, Cyprus, <sup>i</sup>Office of Science, U.S. Department of Energy, Washington, DC 20585, USA, <sup>j</sup>University College Dublin, Dublin 4, Ireland, <sup>k</sup>ETH, 8092 Zurich, Switzerland, <sup>l</sup>University of Fukui, Fukui City, Fukui Prefecture, Japan 910-0017, <sup>m</sup>Universidad Iberoamericana, Mexico D.F., Mexico, <sup>n</sup>University of Iowa, Iowa City, IA 52242, USA, <sup>o</sup>Kinki University, Higashi-Osaka City, Japan 577-8502. <sup>p</sup>Kansas State University, Manhattan, KS 66506.

83  
84  
85  
86  
87  
88  
89  
90  
91  
92  
93  
94  
95  
96  
97  
98  
99  
100  
101  
102  
103  
104  
105  
106  
107  
108  
109

<sup>1</sup>*Institute of Physics, Academia Sinica,  
Taipei, Taiwan 11529, Republic of China*

<sup>2</sup>*Argonne National Laboratory, Argonne, Illinois 60439, USA*

<sup>3</sup>*University of Athens, 157 71 Athens, Greece*

<sup>4</sup>*Institut de Fisica d'Altes Energies, ICREA,  
Universitat Autònoma de Barcelona,  
E-08193, Bellaterra (Barcelona), Spain*

<sup>5</sup>*Baylor University, Waco, Texas 76798, USA*

<sup>6</sup>*Istituto Nazionale di Fisica Nucleare Bologna,  
<sup>ee</sup>University of Bologna, I-40127 Bologna, Italy*

<sup>7</sup>*University of California, Davis, Davis, California 95616, USA*

<sup>8</sup>*University of California, Los Angeles,  
Los Angeles, California 90024, USA*

<sup>9</sup>*Instituto de Fisica de Cantabria, CSIC-University of Cantabria, 39005 Santander, Spain*

<sup>10</sup>*Carnegie Mellon University, Pittsburgh, Pennsylvania 15213, USA*

<sup>11</sup>*Enrico Fermi Institute, University of Chicago, Chicago, Illinois 60637, USA*

<sup>12</sup>*Comenius University, 842 48 Bratislava,  
Slovakia; Institute of Experimental Physics, 040 01 Kosice, Slovakia*

<sup>13</sup>*Joint Institute for Nuclear Research, RU-141980 Dubna, Russia*

<sup>14</sup>*Duke University, Durham, North Carolina 27708, USA*

<sup>15</sup>*Fermi National Accelerator Laboratory, Batavia, Illinois 60510, USA*

<sup>16</sup>*University of Florida, Gainesville, Florida 32611, USA*

<sup>17</sup>*Laboratori Nazionali di Frascati, Istituto Nazionale  
di Fisica Nucleare, I-00044 Frascati, Italy*

<sup>18</sup>*University of Geneva, CH-1211 Geneva 4, Switzerland*

<sup>19</sup>*Glasgow University, Glasgow G12 8QQ, United Kingdom*

<sup>20</sup>*Harvard University, Cambridge, Massachusetts 02138, USA*

---

Kingdom, <sup>s</sup>Queen Mary, University of London, London, E1 4NS, United Kingdom, <sup>t</sup>University of Melbourne, Victoria 3010, Australia, <sup>u</sup>Muons, Inc., Batavia, IL 60510, USA, <sup>v</sup>Nagasaki Institute of Applied Science, Nagasaki, Japan, <sup>w</sup>National Research Nuclear University, Moscow, Russia, <sup>x</sup>Northwestern University, Evanston, IL 60208, USA, <sup>y</sup>University of Notre Dame, Notre Dame, IN 46556, USA, <sup>z</sup>Universidad de Oviedo, E-33007 Oviedo, Spain, <sup>aa</sup>CNRS-IN2P3, Paris, F-75205 France, <sup>bb</sup>Texas Tech University, Lubbock, TX 79609, USA, <sup>cc</sup>Universidad Tecnica Federico Santa Maria, 110v Valparaiso, Chile, <sup>dd</sup>Yarmouk

University, Irbid 211-63, Jordan,

110 <sup>21</sup>*Division of High Energy Physics, Department of Physics,*  
111 *University of Helsinki and Helsinki Institute of Physics, FIN-00014, Helsinki, Finland*  
112 <sup>22</sup>*University of Illinois, Urbana, Illinois 61801, USA*  
113 <sup>23</sup>*The Johns Hopkins University, Baltimore, Maryland 21218, USA*  
114 <sup>24</sup>*Institut für Experimentelle Kernphysik,*  
115 *Karlsruhe Institute of Technology, D-76131 Karlsruhe, Germany*  
116 <sup>25</sup>*Center for High Energy Physics: Kyungpook National University,*  
117 *Daegu 702-701, Korea; Seoul National University, Seoul 151-742,*  
118 *Korea; Sungkyunkwan University, Suwon 440-746,*  
119 *Korea; Korea Institute of Science and Technology Information,*  
120 *Daejeon 305-806, Korea; Chonnam National University, Gwangju 500-757,*  
121 *Korea; Chonbuk National University, Jeonju 561-756, Korea*  
122 <sup>26</sup>*Ernest Orlando Lawrence Berkeley National Laboratory, Berkeley, California 94720, USA*  
123 <sup>27</sup>*University of Liverpool, Liverpool L69 7ZE, United Kingdom*  
124 <sup>28</sup>*University College London, London WC1E 6BT, United Kingdom*  
125 <sup>29</sup>*Centro de Investigaciones Energeticas*  
126 *Medioambientales y Tecnologicas, E-28040 Madrid, Spain*  
127 <sup>30</sup>*Massachusetts Institute of Technology,*  
128 *Cambridge, Massachusetts 02139, USA*  
129 <sup>31</sup>*Institute of Particle Physics: McGill University, Montréal,*  
130 *Québec, Canada H3A 2T8; Simon Fraser University, Burnaby,*  
131 *British Columbia, Canada V5A 1S6; University of Toronto,*  
132 *Toronto, Ontario, Canada M5S 1A7; and TRIUMF,*  
133 *Vancouver, British Columbia, Canada V6T 2A3*  
134 <sup>32</sup>*University of Michigan, Ann Arbor, Michigan 48109, USA*  
135 <sup>33</sup>*Michigan State University, East Lansing, Michigan 48824, USA*  
136 <sup>34</sup>*Institution for Theoretical and Experimental Physics, ITEP, Moscow 117259, Russia*  
137 <sup>35</sup>*University of New Mexico, Albuquerque, New Mexico 87131, USA*  
138 <sup>36</sup>*The Ohio State University, Columbus, Ohio 43210, USA*  
139 <sup>37</sup>*Okayama University, Okayama 700-8530, Japan*  
140 <sup>38</sup>*Osaka City University, Osaka 588, Japan*  
141 <sup>39</sup>*University of Oxford, Oxford OX1 3RH, United Kingdom*

142  
143  
144  
145  
146  
147  
148  
149  
150  
151  
152  
153  
154  
155  
156  
157  
158  
159  
160  
161  
162  
163  
164

<sup>40</sup> *Istituto Nazionale di Fisica Nucleare, Sezione di Padova-Trento,  
ff University of Padova, I-35131 Padova, Italy*

<sup>41</sup> *University of Pennsylvania, Philadelphia, Pennsylvania 19104, USA*

<sup>42</sup> *Istituto Nazionale di Fisica Nucleare Pisa, <sup>99</sup> University of Pisa,  
hh University of Siena and <sup>ii</sup> Scuola Normale Superiore, I-56127 Pisa, Italy*

<sup>43</sup> *University of Pittsburgh, Pittsburgh, Pennsylvania 15260, USA*

<sup>44</sup> *Purdue University, West Lafayette, Indiana 47907, USA*

<sup>45</sup> *University of Rochester, Rochester, New York 14627, USA*

<sup>46</sup> *The Rockefeller University, New York, New York 10065, USA*

<sup>47</sup> *Istituto Nazionale di Fisica Nucleare, Sezione di Roma 1,  
jj Sapienza Università di Roma, I-00185 Roma, Italy*

<sup>48</sup> *Rutgers University, Piscataway, New Jersey 08855, USA*

<sup>49</sup> *Texas A&M University, College Station, Texas 77843, USA*

<sup>50</sup> *Istituto Nazionale di Fisica Nucleare Trieste/Udine,  
I-34100 Trieste, <sup>kk</sup> University of Udine, I-33100 Udine, Italy*

<sup>51</sup> *University of Tsukuba, Tsukuba, Ibaraki 305, Japan*

<sup>52</sup> *Tufts University, Medford, Massachusetts 02155, USA*

<sup>53</sup> *University of Virginia, Charlottesville, Virginia 22906, USA*

<sup>54</sup> *Waseda University, Tokyo 169, Japan*

<sup>55</sup> *Wayne State University, Detroit, Michigan 48201, USA*

<sup>56</sup> *University of Wisconsin, Madison, Wisconsin 53706, USA*

<sup>57</sup> *Yale University, New Haven, Connecticut 06520, USA*

(Dated: November 18, 2011)

## Abstract

165

166 We report on a measurement of  $CP$ -violating asymmetries ( $A_{CP}$ ) in the Cabibbo-suppressed  
167  $D^0 \rightarrow \pi^+\pi^-$  and  $D^0 \rightarrow K^+K^-$  decays reconstructed in a data sample corresponding to  $5.9 \text{ fb}^{-1}$  of  
168 integrated luminosity collected by the upgraded Collider Detector at Fermilab. We use the strong  
169 decay  $D^{*+} \rightarrow D^0\pi^+$  to identify the flavor of the charmed meson at production and exploit  $CP$ -  
170 conserving strong  $c\bar{c}$  pair-production in  $p\bar{p}$  collisions. High-statistics samples of Cabibbo-favored  
171  $D^0 \rightarrow K^-\pi^+$  decays with and without a  $D^{*\pm}$  tag are used to correct for instrumental effects and sig-  
172 nificantly reduce systematic uncertainties. We measure  $A_{CP}(D^0 \rightarrow \pi^+\pi^-) = (+0.22 \pm 0.24 \text{ (stat)} \pm$   
173  $0.11 \text{ (syst)})\%$  and  $A_{CP}(D^0 \rightarrow K^+K^-) = (-0.24 \pm 0.22 \text{ (stat)} \pm 0.09 \text{ (syst)})\%$ , in agreement with  
174  $CP$  conservation. These are the most precise determinations from a single experiment to date. Un-  
175 der the assumption of negligible direct  $CP$  violation in  $D^0 \rightarrow \pi^+\pi^-$  and  $D^0 \rightarrow K^+K^-$  decays, the  
176 results provide an upper limit to the  $CP$ -violating asymmetry in  $D^0$  mixing,  $|A_{CP}^{\text{ind}}(D^0)| < 0.13\%$   
177 at the 90% confidence level.

178 PACS numbers: 13.25.Ft 14.40.Lb

## 179 I. INTRODUCTION

180 The rich phenomenology of neutral flavored mesons provides many experimentally-  
181 accessible observables sensitive to virtual contributions of non-standard model (SM) particles  
182 or couplings. Presence of non-SM physics may alter the expected decay or flavor-mixing  
183 rates, or introduce additional sources of  $CP$  violation besides the Cabibbo-Kobayashi-  
184 Maskawa (CKM) phase. The physics of neutral kaons and bottom mesons has been mostly  
185 explored in dedicated experiments using kaon beams and  $e^+e^-$  collisions [1]. The physics  
186 of bottom-strange mesons is currently being studied in detail in hadron collisions [1]. In  
187 spite of the success of several dedicated experiments in the 1980's and 1990's, experimental  
188 sensitivities to parameters related to mixing and  $CP$  violation in the charm sector were still  
189 orders of magnitude from most SM and non-SM expectations [2]. Improvements from early  
190 measurements at dedicated  $e^+e^-$  colliders at the  $\Upsilon(4S)$  resonance ( $B$ -factories) and the  
191 Tevatron were still insufficient for discriminating among SM and non-SM scenarios [1, 3–6].  
192 Since charm transitions are described by physics of the first two quark generations,  $CP$ -  
193 violating effects are expected to be smaller than  $\mathcal{O}(10^{-2})$ . Thus, relevant measurements  
194 require large event samples and careful control of systematic uncertainties to reach the  
195 needed sensitivity. Also,  $CP$ -violating effects for charm have significantly more uncertain  
196 predictions compared to the bottom and strange sectors because of the intermediate value  
197 of the charm quark mass (too light for factorization of hadronic amplitudes and too heavy  
198 for applying chiral symmetry). All these things taken together have made the advances in  
199 the charm sector slower.

200 Studies of  $CP$  violation in charm decays provide a unique probe for new physics. The  
201 neutral  $D$  system is the only one where up-sector quarks are involved in the initial state.  
202 Thus it probes scenarios where up-type quarks play a special role, such as supersymmetric  
203 models where the down quark and the squark mass matrices are aligned [7, 8] and, more  
204 generally, models in which CKM mixing is generated in the up-quark sector. The interest in  
205 charm dynamics has increased recently with the observation of charm oscillations [9–11]. The  
206 current measurements [3] indicate  $\mathcal{O}(10^{-2})$  magnitudes for the parameters governing their  
207 phenomenology. Such values are on the upper end of most theory predictions [12]. Charm  
208 oscillations could be enhanced by a broad class of non-SM physics processes [13]. Any generic  
209 non-SM contribution to the mixing would naturally carry additional  $CP$ -violating phases,

210 which could enhance the observed  $CP$ -violating asymmetries relative to SM predictions.  
 211 Time integrated  $CP$ -violating asymmetries of singly-Cabibbo-suppressed decays into  $CP$   
 212 eigenstates such as  $D^0 \rightarrow \pi^+\pi^-$  and  $D^0 \rightarrow K^+K^-$  are powerful probes of non-SM physics  
 213 contributions in the “mixing” transition amplitudes. They also probe the magnitude of  
 214 “penguin” contributions, which are negligible in the SM, but could be greatly enhanced by  
 215 the exchange of additional non-SM particles. Both phenomena would, in general, increase the  
 216 size of the observed  $CP$  violation with respect to the SM expectation. Any significant  $CP$ -  
 217 violating asymmetry above the  $10^{-2}$  level expected in the CKM hierarchy would indicate non-  
 218 SM physics. The current experimental status is summarized in Table I. No  $CP$  violation has  
 219 been found within the precision of about 0.5% attained by the Belle and *BABAR* experiments.  
 220 The previous CDF result dates from 2005 and was obtained using data from only  $123 \text{ pb}^{-1}$   
 221 of integrated luminosity. Currently, CDF has the world’s largest samples of exclusive charm  
 222 meson decays in charged final states, with competitive signal purities, owing to the good  
 223 performance of the trigger for displaced tracks. With the current sample CDF can achieve  
 224 a sensitivity that allows probing more extensive portions of the space of non-SM physics  
 225 parameters.

226 We present measurements of time-integrated  $CP$ -violating asymmetries in the Cabibbo-  
 227 suppressed  $D^0 \rightarrow \pi^+\pi^-$  and  $D^0 \rightarrow K^+K^-$  decays (collectively referred to as  $D^0 \rightarrow h^+h^-$   
 228 in this article) using 1.96 TeV proton-antiproton collision data collected by the upgraded  
 229 Collider Detector at Fermilab (CDF II) and corresponding to  $5.9 \text{ fb}^{-1}$  of integrated lumi-  
 230 nosity. Because the final states are common to charm and anti-charm meson decays, the  
 231 time-dependent asymmetry between decays of states identified as  $D^0$  and  $\bar{D}^0$  at the time of  
 232 production ( $t = 0$ ) defined as

$$A_{CP}(h^+h^-, t) = \frac{N(D^0 \rightarrow h^+h^-; t) - N(\bar{D}^0 \rightarrow h^+h^-; t)}{N(D^0 \rightarrow h^+h^-; t) + N(\bar{D}^0 \rightarrow h^+h^-; t)},$$

233 receives contributions from any difference in decay widths between  $D^0$  and  $\bar{D}^0$  mesons in the  
 234 chosen final state (direct  $CP$  violation), any difference in mixing probabilities between  $D^0$   
 235 and  $\bar{D}^0$  mesons, and the interference between direct decays and decays preceded by flavor  
 236 oscillations (both indirect  $CP$  violation). Due to the slow mixing rate of charm mesons, the  
 237 time-dependent asymmetry is approximated at first order as the sum of two terms,

$$A_{CP}(h^+h^-; t) \approx A_{CP}^{\text{dir}}(h^+h^-) + \frac{t}{\tau} A_{CP}^{\text{ind}}(h^+h^-), \quad (1)$$

238 where  $t/\tau$  is the proper decay time in units of  $D^0$  lifetime ( $\tau \approx 0.4$  ps), and the asymmetries  
 239 are related to the decay amplitude  $\mathcal{A}$  and the usual parameters used to describe flavored-  
 240 meson mixing  $x$ ,  $y$ ,  $p$ , and  $q$  [1] by

$$A_{CP}^{\text{dir}}(h^+h^-) \equiv A_{CP}(t=0) = \frac{|\mathcal{A}(D^0 \rightarrow h^+h^-)|^2 - |\mathcal{A}(\bar{D}^0 \rightarrow h^+h^-)|^2}{|\mathcal{A}(D^0 \rightarrow h^+h^-)|^2 + |\mathcal{A}(\bar{D}^0 \rightarrow h^+h^-)|^2}, \quad (2)$$

$$A_{CP}^{\text{ind}}(h^+h^-) = \frac{\eta_{CP}}{2} \left[ y \left( \left| \frac{q}{p} \right| - \left| \frac{p}{q} \right| \right) \cos \varphi - x \left( \left| \frac{q}{p} \right| + \left| \frac{p}{q} \right| \right) \sin \varphi \right], \quad (3)$$

where  $\eta_{CP} = +1$  is the  $CP$ -parity of the decay final state and  $\varphi$  is the  $CP$ -violating phase. The time-integrated asymmetry is then the time integral of Eq. (1) over the observed distribution of proper decay time ( $D(t)$ ),

$$\begin{aligned} A_{CP}(h^+h^-) &= A_{CP}^{\text{dir}}(h^+h^-) + A_{CP}^{\text{ind}}(h^+h^-) \int_0^\infty \frac{t}{\tau} D(t) dt \\ &= A_{CP}^{\text{dir}}(h^+h^-) + \frac{\langle t \rangle}{\tau} A_{CP}^{\text{ind}}(h^+h^-). \end{aligned} \quad (4)$$

241 The first term arises from direct and the second one from indirect  $CP$  violation. Since the  
 242 value of  $\langle t \rangle$  depends on  $D(t)$ , different values of time-integrated asymmetry could be observed  
 243 in different experiments, depending on the detector acceptances as a function of decay time.  
 244 Thus, each experiment may provide different sensitivity to  $A_{CP}^{\text{dir}}$  and  $A_{CP}^{\text{ind}}$ . Since the data  
 245 used in this analysis were collected with an online event selection (trigger) that imposes  
 246 requirements on the displacement of the  $D^0$ -meson decay point from the production point,  
 247 our sample is enriched in higher-valued decay time candidates with respect to experiments  
 248 at the  $B$ -factories. This makes the present measurement more sensitive to mixing-induced  
 249  $CP$  violation. In addition, combination of our results with those from Belle and  $B\bar{B}$ BAR  
 250 provides some discrimination between the two contributions to the asymmetry.

## 251 II. OVERVIEW

252 In the present work we measure the  $CP$ -violating asymmetry in decays of  $D^0$  and  $\bar{D}^0$   
 253 mesons into  $\pi^+\pi^-$  and  $K^+K^-$  final states. Because the final states are charge-symmetric, to  
 254 know whether they originate from a  $D^0$  or a  $\bar{D}^0$  decay, we need the neutral charm candidate  
 255 to be produced in the decay of an identified  $D^{*+}$  or  $D^{*-}$  meson. Flavor conservation in the  
 256 strong-interaction decay of the  $D^{*\pm}$  meson allows identification of the initial charm flavor

TABLE I. Summary of recent experimental measurements of  $CP$ -violating asymmetries. The first quoted uncertainty is statistical, the second uncertainty is systematic.

Experiment	$A_{CP}(\pi^+\pi^-)$ (%)	$A_{CP}(K^+K^-)$ (%)
$B\bar{B}$ 2008 [14]	$-0.24 \pm 0.52 \pm 0.22$	$+0.00 \pm 0.34 \pm 0.13$
Belle 2008 [15]	$-0.43 \pm 0.52 \pm 0.12$	$-0.43 \pm 0.30 \pm 0.11$
CDF 2005 [16]	$+1.0 \pm 1.3 \pm 0.6$	$+2.0 \pm 1.2 \pm 0.6$

through the sign of the charge of the  $\pi$  meson:  $D^{*+} \rightarrow D^0 \pi^+$  and  $D^{*-} \rightarrow \bar{D}^0 \pi^-$ . We refer to  $D$  mesons coming from identified  $D^{*\pm}$  decays as the *tagged* sample and to the tagging pion as the *soft* pion,  $\pi_s$ .

In the data collected by CDF between February 2002 and January 2010, corresponding to an integrated luminosity of about  $5.9 \text{ fb}^{-1}$ , we reconstruct approximately 215 000  $D^{*-}$  tagged  $D^0 \rightarrow \pi^+\pi^-$  decays and 476 000  $D^{*-}$ -tagged  $D^0 \rightarrow K^+K^-$  decays. To measure the asymmetry, we determine the number of detected decays of opposite flavor and use the fact that primary charm and anti-charm mesons are produced in equal numbers by the  $CP$ -conserving strong interaction. The observed asymmetry is the combination of the contributions from  $CP$  violation and from charge asymmetries in the detection efficiency between positive and negative low momentum pions from the  $D^{*\pm}$  decay. To correct for such instrumental asymmetries, which are expected to be of the order of a few  $10^{-2}$ , we use two additional event samples: 5 million tagged, and 29 million untagged Cabibbo-favored  $D^0 \rightarrow K^-\pi^+$  decays. We achieve cancellation of instrumental asymmetries with high accuracy and measure the  $CP$ -violating asymmetries of  $D^0 \rightarrow \pi^+\pi^-$  and  $D^0 \rightarrow K^+K^-$  with a systematic uncertainty of about  $10^{-3}$ .

The paper is structured as follows. In Sec. III we briefly describe the components of the CDF detector relevant for this analysis. In Sec. IV we summarize how the CDF trigger system was used to collect the event sample. We describe the strategy of the analysis and how we correct for detector-induced asymmetries in Sec. V. The event selection and the kinematical requirements applied to isolate the various event samples are presented in Sec. VI; the reweighting of kinematic distributions is discussed in Sec. VII. The determination of observed asymmetries from data is described in Sec. VIII. In Sec. IX we discuss possible sources of systematic uncertainties and finally, in Sec. X, we present the results and compare

281 with measurements performed by other experiments. We also show that by combining the  
 282 present measurement with results from other experiments, we can partially disentangle the  
 283 contribution of direct and indirect  $CP$  violation. A brief summary is presented in Sec. XI. A  
 284 mathematical derivation of the method employed to correct for instrumental asymmetries is  
 285 discussed in Appendix A and its validation on simulated samples is summarized in Appendix  
 286 B.

### 287 III. THE CDF II DETECTOR

288 The CDF II detector has a cylindrical geometry with forward-backward symmetry and  
 289 a tracking system in a 1.4 T magnetic field, coaxial with the beam. The tracking system is  
 290 surrounded by calorimeters [17] and muon-detection chambers [18]. A cylindrical coordinate  
 291 system,  $(r, \phi, z)$ , is used with origin at the geometric center of the detector, where  $r$  is the  
 292 perpendicular distance from the beam,  $\phi$  is the azimuthal angle, and the  $\hat{z}$  vector is in the  
 293 direction of the proton beam. The polar angle  $\theta$  with respect to the proton beam defines  
 294 the pseudorapidity  $\eta$  which is given by  $\eta = -\ln \tan(\theta/2)$ .

295 The CDF II detector tracking system determines the trajectories of charged particles  
 296 (tracks) and consists of an open cell argon-ethane gas drift chamber called the central outer  
 297 tracker (COT) [19] and a silicon vertex microstrip detector (SVX II) [20]. The COT active  
 298 volume covers  $|z| < 155$  cm from a radius of 40 to 140 cm and consists of 96 sense wire layers  
 299 grouped into eight alternating axial and  $2^\circ$  stereo superlayers. To improve the resolution  
 300 on their parameters, tracks found in the COT are extrapolated inward and matched to  
 301 hits in the silicon detector. The SVX II has five layers of silicon strips at radial distances  
 302 ranging from 2.5 cm to 10.6 cm from the beamline. Three of the five layers are double-  
 303 sided planes with  $r - z$  strips oriented at  $90^\circ$  relative to  $r - \phi$  strips, and the remaining  
 304 two layers are double-sided planes with strips oriented at  $\pm 1.2^\circ$  angles relative to the  $r - \phi$   
 305 strips. The SVX II detector consists of three longitudinal barrels, each 29 cm in length,  
 306 and covers approximately 90% of the  $p\bar{p}$  interaction region. The SVX II provides precise  
 307 information on the trajectories of long-lived particles (decay length), which is used for the  
 308 identification of displaced, secondary track vertices of  $B$  and  $D$  hadron decays. An innermost  
 309 single-sided silicon layer (L00), installed at 1.5 cm from the beam, further improves the  
 310 resolution for vertex reconstruction [21]. Outside of the SVX II, two additional layers of

311 silicon assist pattern recognition and extend the sensitive region of the tracking detector to  
 312  $|\eta| \approx 2$  [22]. These intermediate silicon layers (ISL) are located between the SVX II and  
 313 the COT and consist of one layer at a radius of 23 cm in the central region,  $|\eta| \leq 1$ , and  
 314 two layers in the forward region  $1 \leq |\eta| \leq 2$ , at radii of 20 and 29 cm. The component of a  
 315 charged particle's momentum transverse to the beam ( $p_T$ ) is determined with a resolution of  
 316  $\sigma_{p_T}/p_T \approx 0.07\% p_T$  ( $p_T$  in GeV/ $c$ ) for tracks with  $p_T > 2$  GeV/ $c$ . The excellent momentum  
 317 resolution yields precise mass resolution, which provides good signal-to-background for fully  
 318 reconstructed  $B$  and  $D$  decay modes. The typical resolution on the reconstructed position of  
 319 decay vertices is approximately  $30 \mu\text{m}$  in the transverse direction, effective to identify vertices  
 320 from charmed meson decays, which are typically displaced by  $250 \mu\text{m}$  from the beam. In  
 321 the longitudinal direction, the resolution is approximately  $70 \mu\text{m}$ , allowing suppression of  
 322 backgrounds from charged particles originating from decays of distinct heavy hadrons in the  
 323 event.

#### 324 IV. ONLINE SAMPLE SELECTION

325 The CDF II trigger system is a key element that makes this measurement possible.  
 326 Identification of hadronic decays of heavy-flavored mesons is challenging in the Tevatron  
 327 collider environment due to the large inelastic  $p\bar{p}$  cross section and high particle multiplicities  
 328 at 1.96 TeV. In order to collect these events, the trigger system must reject more than 99.99%  
 329 of the collisions while retaining good efficiency for signal. In this Section, we describe the  
 330 CDF II trigger system and the algorithms used in collecting the samples of hadronic  $D$   
 331 decays in this analysis.

332 The CDF II trigger system has a three-level architecture: the first two levels, level 1 (L1)  
 333 and level 2 (L2), are implemented in hardware and the third, level 3 (L3), is implemented in  
 334 software on a cluster of computers using reconstruction algorithms that are similar to those  
 335 used off line.

336 Using information from the COT, at L1, the extremely fast tracker (XFT) [23] recon-  
 337 structs trajectories of charged particles in the  $r - \phi$  plane for each proton-antiproton bunch  
 338 crossing. Events are selected for further processing when two tracks that satisfy trigger  
 339 criteria on basic variables are found. The variables include the product of any combination  
 340 of two particles' charges (opposite or same sign), the opening angle of the two tracks in the

341 transverse plane ( $\Delta\phi$ ), the two particles' transverse momenta, and their scalar sum.

342 At L2 the silicon vertex trigger (SVT) [24] incorporates information from the SVX II  
343 detector into the trigger track reconstruction. The SVT identifies tracks displaced from the  
344  $p\bar{p}$  interaction point, such as those that arise from weak decays of heavy hadrons and have  
345 sufficient transverse momentum. Displaced tracks are those that have a distance of closest  
346 approach to the beamline (impact parameter  $d_0$ ) inconsistent with having originated from  
347 the  $p\bar{p}$  interaction point (primary vertex). The impact parameter resolution of the SVT  
348 is approximately  $50\ \mu\text{m}$ , which includes a contribution of  $35\ \mu\text{m}$  from the width of the  $p\bar{p}$   
349 interaction region. The trigger selections used in this analysis typically require two tracks,  
350 each with impact parameter greater than  $120\ \mu\text{m}$  and smaller than  $1\ \text{mm}$ . In addition,  
351 the L2 trigger requires the transverse decay length ( $L_{xy}$ ) to exceed  $200\ \mu\text{m}$ , where  $L_{xy}$  is  
352 calculated as the projection of the vector from the primary vertex to the two-track vertex  
353 in the transverse plane along the vectorial sum of the transverse momenta of the tracks.  
354 The trigger based on the SVT collects large quantities of long-lived  $D$  hadrons, rejecting  
355 most of the prompt background. However, through its impact-parameter-based selection,  
356 the SVT trigger also biases the observed proper decay time distribution. This has important  
357 consequences for the results of this analysis, which will be discussed in Sec. X.

358 The L3 trigger uses a full reconstruction of the event with all detector information, but  
359 uses a simpler tracking algorithm and preliminary calibrations relative to the ones used off  
360 line. The L3 trigger retests the criteria imposed by the L2 trigger. In addition, the difference  
361 in  $z$  of the two tracks at the point of minimum distance from the primary vertex,  $\Delta z_0$ , is  
362 required not to exceed  $5\ \text{cm}$ , removing events where the pair of tracks originate from different  
363 collisions within the same crossing of  $p$  and  $\bar{p}$  bunches.

364 Over the course of a single continuous period of Tevatron collisions (a store), the available  
365 trigger bandwidth varies because trigger rates fall as instantaneous luminosity falls. Higher  
366 trigger rates at high luminosity arise from both a larger rate for real physics processes as well  
367 as multiplicity-dependent backgrounds in multiple  $p\bar{p}$  interactions. To fully exploit the avail-  
368 able trigger bandwidth, we employ three main variants of the displaced-tracks trigger. The  
369 three selections are summarized in Table II and are referred to as the low- $p_T$ , medium- $p_T$ ,  
370 and high- $p_T$  selections according to their requirements on minimum transverse momentum.  
371 At high luminosity, the higher purity but less efficient, high- $p_T$  selection is employed. As  
372 the luminosity decreases over the course of a store, trigger bandwidth becomes available and

TABLE II. Typical selection criteria for the three versions of the displaced-tracks trigger used in this analysis. The criteria refer to track pairs. The  $p_T$ ,  $d_0$ , and  $\eta$  requirements are applied to both tracks. The  $\sum p_T$  refers to the scalar sum of the  $p_T$  of the two tracks. The  $\sum p_T$  threshold in each of the three vertical portions of the table identifies the high- $p_T$  (top), medium- $p_T$  (middle), and low- $p_T$  (bottom) trigger selections.

Level-1	Level-2	Level-3
$p_T > 2.5 \text{ GeV}/c$	$p_T > 2.5 \text{ GeV}/c$	$p_T > 2.5 \text{ GeV}/c$
$\sum p_T > 6.5 \text{ GeV}/c$	$\sum p_T > 6.5 \text{ GeV}/c$	$\sum p_T > 6.5 \text{ GeV}/c$
Opposite charge	Opposite charge	Opposite charge
$\Delta\phi < 90^\circ$	$2^\circ < \Delta\phi < 90^\circ$	$2^\circ < \Delta\phi < 90^\circ$
	$0.12 < d_0 < 1.0 \text{ mm}$	$0.1 < d_0 < 1.0 \text{ mm}$
	$L_{xy} > 200 \mu\text{m}$	$L_{xy} > 200 \mu\text{m}$
		$ \Delta z_0  < 5 \text{ cm}$
		$ \eta  < 1.2$
$p_T > 2 \text{ GeV}/c$	$p_T > 2 \text{ GeV}/c$	$p_T > 2 \text{ GeV}/c$
$\sum p_T > 5.5 \text{ GeV}/c$	$\sum p_T > 5.5 \text{ GeV}/c$	$\sum p_T > 5.5 \text{ GeV}/c$
Opposite charge	Opposite charge	Opposite charge
$\Delta\phi < 90^\circ$	$2^\circ < \Delta\phi < 90^\circ$	$2^\circ < \Delta\phi < 90^\circ$
	$0.12 < d_0 < 1.0 \text{ mm}$	$0.1 < d_0 < 1.0 \text{ mm}$
	$L_{xy} > 200 \mu\text{m}$	$L_{xy} > 200 \mu\text{m}$
		$ \Delta z_0  < 5 \text{ cm}$
		$ \eta  < 1.2$
$p_T > 2 \text{ GeV}/c$	$p_T > 2 \text{ GeV}/c$	$p_T > 2 \text{ GeV}/c$
$\sum p_T > 4 \text{ GeV}/c$	$\sum p_T > 4 \text{ GeV}/c$	$\sum p_T > 4 \text{ GeV}/c$
$\Delta\phi < 90^\circ$	$2^\circ < \Delta\phi < 90^\circ$	$2^\circ < \Delta\phi < 90^\circ$
	$0.1 < d_0 < 1.0 \text{ mm}$	$0.1 < d_0 < 1.0 \text{ mm}$
	$L_{xy} > 200 \mu\text{m}$	$L_{xy} > 200 \mu\text{m}$
		$ \Delta z_0  < 5 \text{ cm}$
		$ \eta  < 1.2$

373 the other selections are utilized to fill the available trigger bandwidth and maximize the  
 374 charm yield. The rates are controlled by the application of a prescale, which rejects a prede-  
 375 fined fraction of events accepted by each trigger selection, depending on the instantaneous  
 376 luminosity.

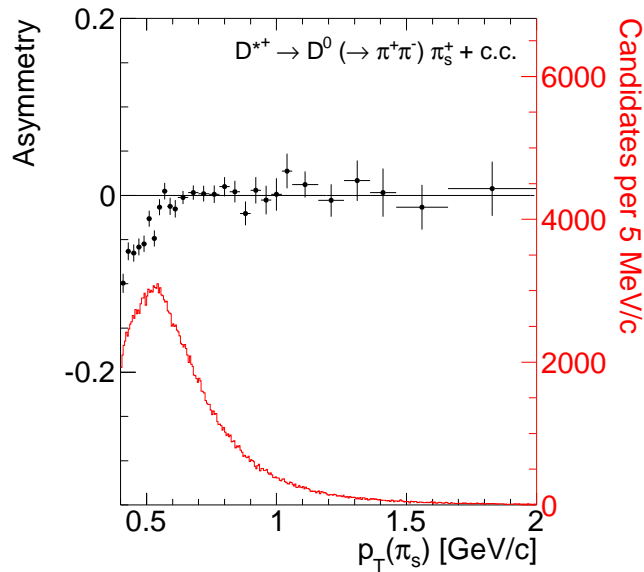
## 377 V. SUPPRESSING DETECTOR-INDUCED CHARGE ASYMMETRIES

378 The procedure used to cancel detector-induced asymmetries is briefly outlined here, while  
 379 a detailed mathematical treatment is given in Appendix A.

380 We directly measure the observed “raw” asymmetry:

$$A(D^0) = \frac{N_{\text{obs}}(D^0) - N_{\text{obs}}(\overline{D}^0)}{N_{\text{obs}}(D^0) + N_{\text{obs}}(\overline{D}^0)},$$

381 that is, the number of observed  $D^0$  decays into the selected final state ( $\pi^+\pi^-$  or  $K^+K^-$ )  
 382 minus the number of  $\overline{D}^0$  decays, divided by the sum.



383

384 FIG. 1. Observed asymmetry between the number of reconstructed  $D^{*+}$  and  $D^{*-}$  mesons as a  
 385 function of the soft pion’s transverse momentum for pure samples of  $D^{*+} \rightarrow D^0(\rightarrow \pi^+\pi^-)\pi_s^+$  and  
 386  $D^{*-} \rightarrow \overline{D}^0(\rightarrow \pi^+\pi^-)\pi_s^-$  decays. The soft pion transverse momentum spectrum is also shown.

387 The main experimental difficulty of this measurement comes from the small differences in  
 388 the detection efficiencies of tracks of opposite charge which may lead, if not properly taken

389 into account, to spuriously-measured charge asymmetries. Relevant instrumental effects  
 390 include differences in interaction cross sections with matter between positive and negative  
 391 low-momentum hadrons and the geometry of the main tracking system. The drift chamber  
 392 layout is intrinsically charge asymmetric because of a  $\approx 35^\circ$  tilt angle between the cell  
 393 orientation and the radial direction, designed to partially correct for the Lorentz angle in the  
 394 charge drift direction caused by crossed electric and magnetic fields. In the COT, different  
 395 detection efficiencies are expected for positive and negative low-momentum tracks (especially,  
 396 in our case, for soft pions), which induce an instrumental asymmetry in the number of  
 397 reconstructed  $D^*$ -tagged  $D^0$  and  $\bar{D}^0$  mesons. Other possible asymmetries may originate in  
 398 slightly different performance between positive and negative tracks in pattern-reconstruction  
 399 and track-fitting algorithms. The combined effect of these is a net asymmetry in the range  
 400 of a few percent, as shown in Fig. 1. This must be corrected to better than one per mil  
 401 to match the expected statistical precision of the present measurement. In order to cancel  
 402 detector effects, we extract the value of  $A_{CP}(D^0 \rightarrow h^+h^-)$  using a fully data-driven method,  
 403 based on an appropriate combination of charge-asymmetries observed in three different event  
 404 samples:  $D^*$ -tagged  $D^0 \rightarrow h^+h^-$  decays (or simply  $hh^*$ ),  $D^*$ -tagged  $D^0 \rightarrow K^-\pi^+$  decays  
 405 ( $K\pi^*$ ), and untagged  $D^0 \rightarrow K^-\pi^+$  decays ( $K\pi$ ). We assume the involved physical and  
 406 instrumental asymmetries to be small, as indicated by previous measurements. Neglecting  
 407 terms of order  $A_{CP}\delta$  and  $\delta^2$ , the observed asymmetries in the three samples are

$$\begin{aligned}
 A(hh^*) &= A_{CP}(hh) + \delta(\pi_s)^{hh^*}, \\
 A(K\pi^*) &= A_{CP}(K\pi) + \delta(\pi_s)^{K\pi^*} + \delta(K\pi)^{K\pi^*}, \\
 A(K\pi) &= A_{CP}(K\pi) + \delta(K\pi)^{K\pi},
 \end{aligned}
 \tag{5}$$

408 where  $\delta(\pi_s)^{hh^*}$  is the instrumental asymmetry for reconstructing a positive or negative soft  
 409 pion associated with a  $h^+h^-$  charm decay induced by charge-asymmetric interaction cross  
 410 section and reconstruction efficiency for low transverse momentum pions;  $\delta(\pi_s)^{K\pi^*}$  is the  
 411 same as above for tagged  $K^+\pi^-$  and  $K^-\pi^+$  decays; and  $\delta(K\pi)^{K\pi}$  and  $\delta(K\pi)^{K\pi^*}$  are the  
 412 instrumental asymmetries for reconstructing a  $K^+\pi^-$  or a  $K^-\pi^+$  decay for the untagged  
 413 and the tagged case, respectively. All the above effects can vary as functions of a number  
 414 of kinematic variables or environmental conditions in the detector. If the kinematic dis-  
 415 tributions of soft pions are consistent in  $K\pi^*$  and  $hh^*$  samples, and if the distributions of  
 416  $D^0$  decay products are consistent in  $K\pi^*$  and  $K\pi$  samples, then  $\delta(\pi_s)^{hh^*} \approx \delta(\pi_s)^{K\pi^*}$  and

417  $\delta(K\pi)^{K\pi^*} \approx \delta(K\pi)^{K\pi}$ . The  $CP$ -violating asymmetries then become accessible as

$$A_{CP}(hh) = A(hh^*) - A(K\pi^*) + A(K\pi). \quad (6)$$

418 This formula relies on cancellations based on two assumptions. At the Tevatron, charm  
 419 and anticharm mesons are expected to be created in almost equal numbers. Since the  
 420 overwhelming majority of them are produced by  $CP$ -conserving strong interactions, and the  
 421  $p\bar{p}$  initial state is  $CP$  symmetric, any small difference between the abundance of charm and  
 422 anti-charm flavor is constrained to be antisymmetric in pseudorapidity. As a consequence,  
 423 we assume that the net effect of any possible charge asymmetry in the production cancels  
 424 out, as long as the distribution of the decays in the sample used for this analysis is symmetric  
 425 in pseudorapidity. An upper limit to any possible residual effect is evaluated as part of the  
 426 study of systematic uncertainties (Sec. IX). The second assumption is that the detection  
 427 efficiency for the  $D^*$  can be expressed as the product of the efficiency for the soft pion times  
 428 the efficiency for the  $D^0$  final state. This assumption has been tested (Sec. IX), and any  
 429 residual effect included in the systematic uncertainties.

430 Before applying this technique to data, we show that our approach achieves the goal of  
 431 suppressing detector induced asymmetries down to the per mil level using the full Monte  
 432 Carlo simulation (Appendix B). The simulation contains only charmed signal decays. The  
 433 effects of the underlying event and multiple interactions are not simulated. We apply the  
 434 method to samples simulated with a wide range of physical and detector asymmetries to  
 435 verify that the cancellation works. The simulation is used here only to test the validity of the  
 436 technique; all final results are derived from data only, with no direct input from simulation.

## 437 VI. ANALYSIS EVENT SELECTION

438 The offline selection is designed to retain the maximum number of  $D^0 \rightarrow h^+h'^-$  decays  
 439 with accurately measured momenta and decay vertices. Any requirements that may induce  
 440 asymmetries between the number of selected  $D^0$  and  $\bar{D}^0$  mesons are avoided. The recon-  
 441 struction is based solely on tracking, disregarding any information on particle identification.  
 442 Candidate decays are reconstructed using only track pairs compatible with having fired the  
 443 trigger. Standard quality criteria on the minimum number of associated silicon-detector  
 444 and drift-chamber hits are applied to each track to ensure precisely measured momenta and

445 decay vertices in three-dimensions [25]. Each final-state particle is required to have  $p_T > 2.2$   
 446  $\text{GeV}/c$ ,  $|\eta| < 1$ , and impact parameter between 0.1 and 1 mm. The reconstruction of  $D^0$   
 447 candidates considers all pairs of oppositely-charged particles in an event, which are arbi-  
 448 trarily assigned the charged pion mass. The two tracks are constrained to originate from a  
 449 common vertex by a kinematic fit subject to standard quality requirements. The  $\pi^+\pi^-$  mass  
 450 of candidates is required to be in the range 1.8 to 2.4  $\text{GeV}/c^2$ , to retain all signals of interest  
 451 and sideband regions sufficiently wide to study backgrounds. The two tracks are required  
 452 to have an azimuthal separation  $2^\circ < \Delta\phi < 90^\circ$ , and correspond to a scalar sum of the two  
 453 particles' transverse momenta greater than 4.5  $\text{GeV}/c$ . We require  $L_{xy}$  to exceed 200  $\mu\text{m}$  to  
 454 reduce background from decays of hadrons that don't contain heavy quarks. We also require  
 455 the impact parameter of the  $D^0$  candidate with respect to the beam,  $d_0(D^0)$ , to be smaller  
 456 than 100  $\mu\text{m}$  to reduce the contribution from charmed mesons produced in long-lived  $B$   
 457 decays (secondary charm). In the rare (0.04%) occurrence that multiple  $D^0 \rightarrow h^+h'^-$  decays  
 458 sharing the same tracks are reconstructed in the event, we retain the one having the best  
 459 vertex fit quality.

461 Figure 2 shows the  $K^-\pi^+$  mass distribution for the resulting sample, which is referred  
 462 to as “untagged” in the following since no  $D^*$  decay reconstruction has been imposed at  
 463 this stage. The distribution of a sample of simulated inclusive charmed decays is also shown  
 464 for comparison. Only a single charmed meson decay per event is simulated without the  
 465 underlying event. In both distributions the kaon (pion) mass is arbitrarily assigned to the  
 466 negative (positive) particle. The prominent narrow signal is dominated by  $D^0 \rightarrow K^-\pi^+$  de-  
 467 cays. A broader structure, also centered on the known  $D^0$  mass, are  $\bar{D}^0 \rightarrow K^+\pi^-$  candidates  
 468 reconstructed with swapped  $K$  and  $\pi$  mass assignments to the decay products. Approxi-  
 469 mately 29 million  $D^0$  and  $\bar{D}^0$  mesons decaying into  $K^\pm\pi^\mp$  final states are reconstructed.  
 470 The two smaller enhancements at lower and higher masses than the  $D^0$  signal are due to  
 471 mis-reconstructed  $D^0 \rightarrow K^+K^-$  and  $D^0 \rightarrow \pi^+\pi^-$  decays, respectively. Two sources of  
 472 background contribute. A component of random track pairs that accidentally meet the  
 473 selection requirements (combinatorial background) is most visible at masses higher than 2  
 474  $\text{GeV}/c^2$ , but populates almost uniformly the whole mass range. A large shoulder due to  
 475 mis-reconstructed multi-body charm decays peaks at a mass of approximately 1.6  $\text{GeV}/c^2$ .

476 In the “tagged”-samples reconstruction, we form  $D^{*+} \rightarrow D^0\pi_s^+$  candidates by associating  
 477 with each  $D^0$  candidate all tracks present in the same event. The additional particle is

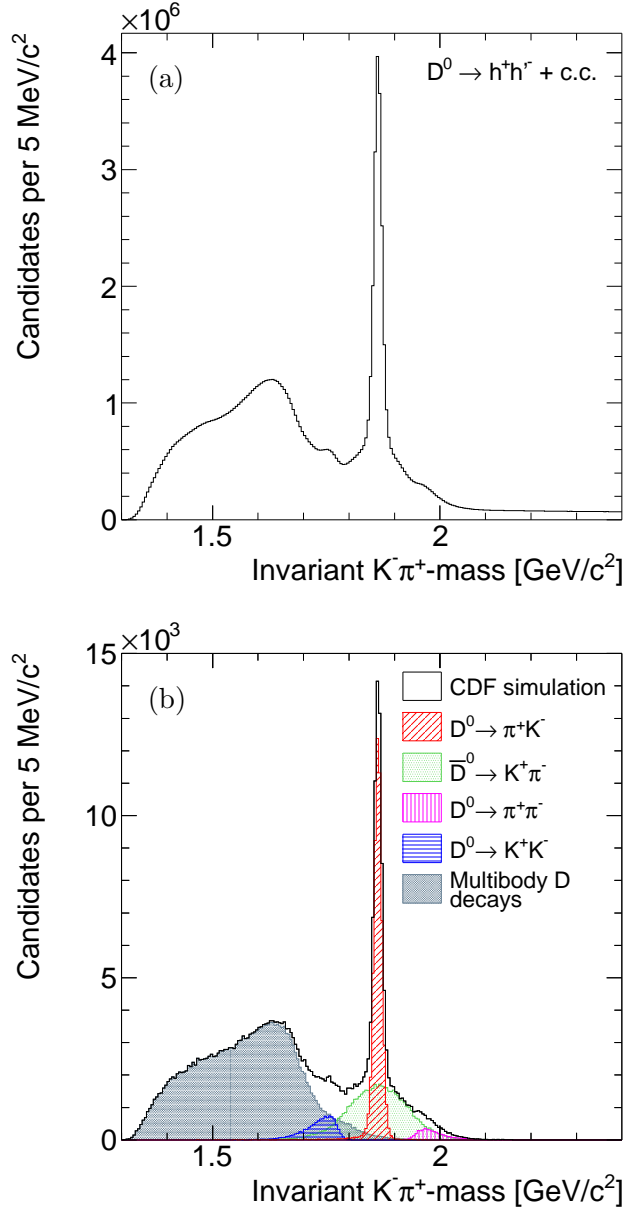


FIG. 2. Comparison between the  $K^-\pi^+$ -mass distributions of (a) the untagged sample and of (b) a simulated sample of inclusive charm decays. See text for explanation of contributions.

478 required to satisfy basic quality requirements for the numbers of associated silicon and  
 479 drift chamber hits, to be central ( $|\eta| < 1$ ), and to have transverse momentum greater than  
 480 400  $\text{MeV}/c$ . We assume this particle to be a pion (“soft pion”) and we match its trajectory  
 481 to the  $D^0$  vertex with simple requirements on relative separation: impact parameter smaller  
 482 than 600  $\mu\text{m}$  and longitudinal distance from the primary vertex smaller than 1.5 cm. Since  
 483 the impact parameter of the low-energy pion has degraded resolution with respect to those

484 of the  $D^0$  tracks, no real benefit is provided by a full three-track vertex fit for the  $D^*$   
 485 candidate. We retain  $D^*$  candidates with  $D^0\pi_s$  mass smaller than  $2.02 \text{ GeV}/c^2$ . In the  
 486 2% of cases in which multiple  $D^*$  candidates are associated with a single  $D^0$  candidate, we  
 487 randomly choose only one  $D^*$  candidate for further analysis.

488 The  $D^0\pi_s$  mass is calculated using the vector sum of the momenta of the three particles as  
 489  $D^*$  momentum, and the known  $D^0$  mass in the determination of the  $D^*$  energy. This quantity  
 490 has the same resolution advantages of the more customary  $M(h^+h^{(\prime)-}\pi_s) - M(h^+h^{(\prime)-})$  mass  
 491 difference, and has the additional advantage that it is independent of the mass assigned to  
 492 the  $D^0$  decay products. Therefore all  $D^{*+} \rightarrow D^0(\rightarrow h^+h^{(\prime)-})\pi_s^+$  modes have the same  $D^0\pi_s$   
 493 mass distribution, which is not true for the mass difference distribution.

494 In each tagged sample ( $D^0 \rightarrow \pi^+\pi^-$ ,  $D^0 \rightarrow K^+K^-$  and  $D^0 \rightarrow K^-\pi^+$ ) we require  
 495 the corresponding two-body mass to lie within  $24 \text{ MeV}/c^2$  of the known  $D^0$  mass [1], as  
 496 shown in Figs. 3 (a)–(c). Figures 3 (d)–(f) show the resulting  $D^0\pi_s$  mass distribution. A  
 498 clean  $D^*$  signal is visible superimposed on background components that are different in each  
 499  $D^0$  channel. As will be shown in Sec. VIII, the backgrounds in the  $D^0\pi_s$  distributions for  
 500  $D^0 \rightarrow \pi^+\pi^-$  and  $D^0 \rightarrow K^+K^-$  decays are mainly due to associations of random pions with  
 501 real  $D^0$  candidates. In the  $D^0 \rightarrow K^+K^-$  case, there is also a substantial contribution from  
 502 mis-reconstructed multi-body charged and neutral charmed decays (mainly  $D^{*+} \rightarrow D^0(\rightarrow$   
 503  $K^-\pi^+\pi^0)\pi_s^+$  where the neutral pion is not reconstructed) that yield a broader enhancement  
 504 underneath the signal peak. We reconstruct approximately 215 000  $D^*$ -tagged  $D^0 \rightarrow \pi^+\pi^-$   
 505 decays, 476 000  $D^*$ -tagged  $D^0 \rightarrow K^+K^-$  decays, and 5 million  $D^*$ -tagged  $D^0 \rightarrow \pi^+K^-$   
 506 decays.

## 507 VII. KINEMATIC DISTRIBUTIONS EQUALIZATION

508 Because detector-induced asymmetries depend on kinematic properties, the asymmetry  
 509 cancellation is realized accurately only if the kinematic distributions across the three sam-  
 510 ples are the same. Although the samples have been selected using the same requirements,  
 511 small kinematic differences between decay channels may persist due to the different masses  
 512 involved. We extensively search for any such residual effect across several kinematic distri-  
 513 butions and reweight the tagged  $D^0 \rightarrow h^+h^-$  and untagged  $D^0 \rightarrow K^-\pi^+$  distributions to  
 514 reproduce the tagged  $D^0 \rightarrow K^-\pi^+$  distributions when necessary. For each channel, identical

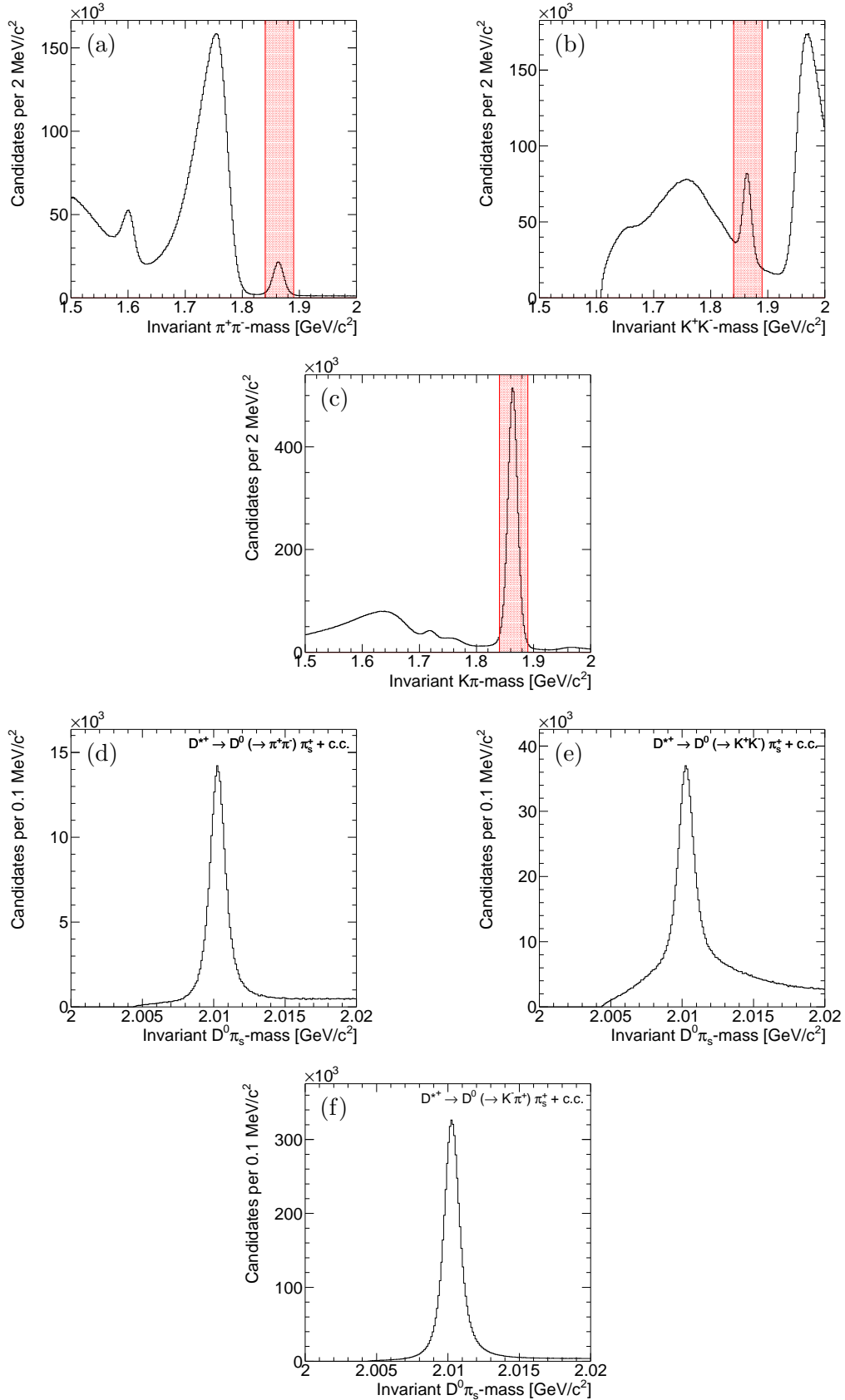


FIG. 3. Distributions of (a)  $\pi^+\pi^-$ , (b)  $K^+K^-$ , and (c)  $K\pi$  mass. Regions used to define the tagged samples are shaded. Distribution of  $D^0\pi_s$  mass for tagged (d)  $D^0 \rightarrow \pi^+\pi^-$ , (e)  $D^0 \rightarrow K^+K^-$ , and (f)  $D^0 \rightarrow K^-\pi^+$  samples selected in the shaded regions.

515 reweighting functions are used for charm and anti-charm decays.

516 We define appropriate sideband regions according to the specific features of each tagged  
517 sample (Fig. 3 (a)–(c)). Then we compare background-subtracted distributions for tagged  
518  $h^+h^{(\prime)-}$  decays, studying a large set of  $\pi_s$  kinematic variables ( $p_T$ ,  $\eta$ ,  $\phi$ ,  $d_0$ , and  $z_0$ ) [25]. We  
519 observe small discrepancies only in the transverse momentum and pseudorapidity distribu-  
520 tions as shown in Fig. 4 (a)–(d). The ratio between the two distributions is used to extract  
521 a smooth curve used as a candidate-specific weight. A similar study of  $D^0$  distributions for  
522 tagged and untagged  $D^0 \rightarrow K^-\pi^+$  decays shows discrepancies only in the distributions of  
523 transverse momentum and pseudorapidity (Fig. 4) which are reweighted accordingly.

524 Background is not subtracted from the distributions of the untagged sample. We simply  
525 select decays with  $K^+\pi^-$  or  $K^-\pi^+$ -mass within 24 MeV/ $c^2$  from the known  $D^0$  mass, cor-  
526 responding approximately to a cross-shaped  $\pm 3\sigma$  range in the two-dimensional distribution  
527 (Fig. 5). The background contamination in this region is about 6%. This contamination  
528 has a small effect on the final result. The observed asymmetries show a small dependence  
529 on the  $D^0$  momentum, because detector-induced charge asymmetries are tiny at transverse  
530 momenta greater than 2.2 GeV/ $c$ , as required for the  $D^0$  decay products. Therefore any  
531 small imperfection in the reweighting of momentum spectra between tagged and untagged  
532 sample has a limited impact, if any. However, a systematic uncertainty is assessed for the  
533 possible effects of non-subtracted backgrounds (see Sec. IX). All entries in distributions  
534 shown in the remainder of this paper are reweighted according to the transverse momentum  
535 and pseudorapidity of the corresponding candidates unless otherwise stated.

## 536 VIII. DETERMINATION OF OBSERVED ASYMMETRIES

537 The asymmetries between observed numbers of  $D^0$  and  $\bar{D}^0$  signal candidates are deter-  
538 mined with fits of the  $D^*$  (tagged samples) and  $D^0$  (untagged sample) mass distributions.  
539 The mass resolution of the CDF tracker is sufficient to separate the different decay modes  
540 of interest. Backgrounds are modeled and included in the fits. In all cases we use a joint  
541 binned fit that minimizes a combined  $\chi^2$  quantity, defined as  $\chi_{\text{tot}}^2 = \chi_+^2 + \chi_-^2$ , where  $\chi_+^2$  and  
542  $\chi_-^2$  are the individual  $\chi^2$  for the  $D^0$  and  $\bar{D}^0$  distributions. Because we use copious samples,  
543 an unbinned likelihood fit would imply a substantially larger computational load without  
544 a significant improvement in statistical resolution. The functional form that describes the

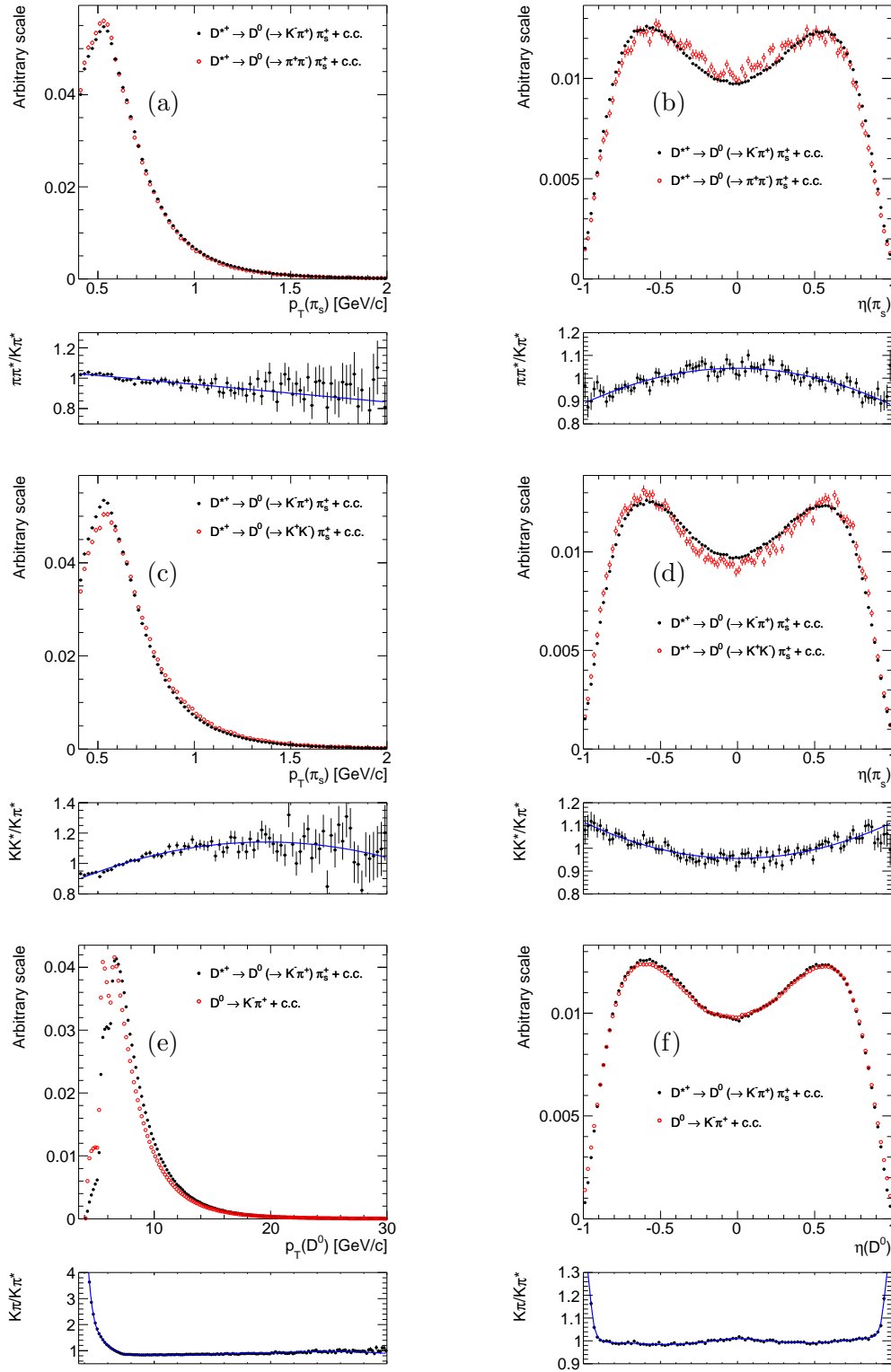


FIG. 4. Comparison between normalized kinematic distributions of the various tagged and untagged samples used in the analysis: (a), (c) soft pion transverse momentum, and (b),(d) pseudo-rapidity of  $hh^*$  and  $K\pi^*$  events; (e)  $D^0$  transverse momentum and (f) pseudorapidity of  $K\pi$  and  $K\pi^*$  events. Tagged distributions are background-subtracted.

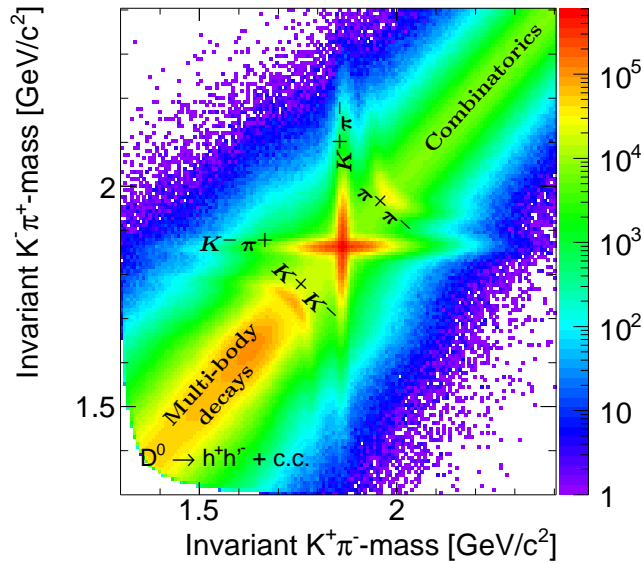


FIG. 5. Distribution of  $K^- \pi^+$ -mass as a function of  $K^+ \pi^-$ -mass for the untagged sample. Note the logarithmic scale on  $z$  axis.

545 mass shape is assumed to be the same for charm and anti-charm, although a few parameters  
 546 are determined by the fit independently in the two samples. The functional form of the  
 547 mass shape for all signals is extracted from simulation and the values of its parameters ad-  
 548 justed for the data. The effect of this adjustment is discussed in Sec. IX where a systematic  
 549 uncertainty is also assessed.

### 550 A. Fit of tagged samples

551 We extract the asymmetry of tagged samples by fitting the numbers of reconstructed  
 552  $D^{*\pm}$  events in the  $D^0 \pi_s^+$  and  $\bar{D}^0 \pi_s^-$  mass distribution. Because all  $D^0 \rightarrow h^+ h'^-$  modes have  
 553 the same  $D^0 \pi_s^+$  mass distribution, we use a single shape to fit all tagged signals. We also  
 554 assume that the shape of the background from random pions associated with a real neutral  
 555 charm particle are the same. Systematic uncertainties due to variations in the shapes are  
 556 discussed later in Sec. IX.

557 The general features of the signal distribution are extracted from simulated samples.  
 558 The model is adjusted and finalized in a fit of the  $D^0 \pi_s$  mass of copious and pure tagged  
 559  $K^- \pi^+$  decays. We fit the average histogram of the charm and anti-charm samples,  $m =$

560  $(m_+ + m_-)/2$ , where  $m_+$  is the  $D^{*+}$  mass distribution and  $m_-$  the  $D^{*-}$  one. The resulting  
 561 signal shape is then used in the joint fit to measure the asymmetry between charm and  
 562 anti-charm signal yields. The signal is described by a Johnson function [26] (all functions  
 563 properly normalized in the appropriate fit range),

$$J(x|\mu, \sigma, \delta, \gamma) = \frac{e^{-\frac{1}{2}[\gamma + \delta \sinh^{-1}(\frac{x-\mu}{\sigma})]^2}}{\sqrt{1 + (\frac{x-\mu}{\sigma})^2}},$$

that accounts for the asymmetric tail of the distribution, plus two Gaussians,  $\mathcal{G}(x|\mu, \sigma)$ , for  
 the central bulk:

$$\begin{aligned} \wp_{\text{sig}}(m|\vec{\theta}_{\text{sig}}) = & f_J J(m|m_{D^*} + \mu_J, \sigma_J, \delta_J, \gamma_J) + (1 - f_J) \\ & \times [f_{G1} \mathcal{G}(m|m_{D^*} + \mu_{G1}, \sigma_{G1}) \\ & + (1 - f_{G1}) \mathcal{G}(m|m_{D^*} + \mu_{G2}, \sigma_{G2})]. \end{aligned}$$

564 The signal parameters  $\vec{\theta}_{\text{sig}}$  include the relative fractions between the Johnson and the Gaus-  
 565 sian components; the shift from the nominal  $D^{*\pm}$  mass of the Johnson distribution's core,  
 566  $\mu_J$ , and the two Gaussians,  $\mu_{G1(2)}$ ; the widths of the Johnson distribution's core,  $\sigma_J$ , and  
 567 the two Gaussians,  $\sigma_{G1(2)}$ ; and the parameters  $\delta_J$  and  $\gamma_J$ , which determine the asymmetry  
 568 in the Johnson distribution's tails. For the random pion background we use an empirical  
 569 shape form,

$$\wp_{\text{bkg}}(m|\vec{\theta}_{\text{bkg}}) = \mathcal{B}(m|m_{D^0} + m_\pi, b_{\text{bkg}}, c_{\text{bkg}}),$$

570 with  $\mathcal{B}(x|a, b, c) = (x - a)^b e^{-c(x-a)}$  extracted from data by forming an artificial random  
 571 combination made of a well-reconstructed  $D^0$  meson from each event combined with pions  
 572 from all other events. The total function used in this initial fit is

$$N_{\text{sig}} \wp_{\text{sig}}(m|\vec{\theta}_{\text{sig}}) + N_{\text{bkg}} \wp_{\text{bkg}}(m|\vec{\theta}_{\text{bkg}}).$$

573 Each fit function is defined only above the threshold value of  $m_{D^0} + m_\pi$ . Figure 6 shows  
 575 the resulting fit which is used to determine the shape parameters for subsequent asymmetry  
 576 fits. All parameters are free to float in the fit.

578 We then fix the signal parametrization and simultaneously fit the  $D^0\pi_s$  mass distributions  
 579 of  $D^{*+}$  and  $D^{*-}$  candidates with independent normalizations to extract the asymmetry. The  
 580 parameter  $\delta_J$  varies independently for charm and anti-charm decays. The background shape  
 581 parameters are common in the two samples and are determined by the fit. Figures 7 (a)

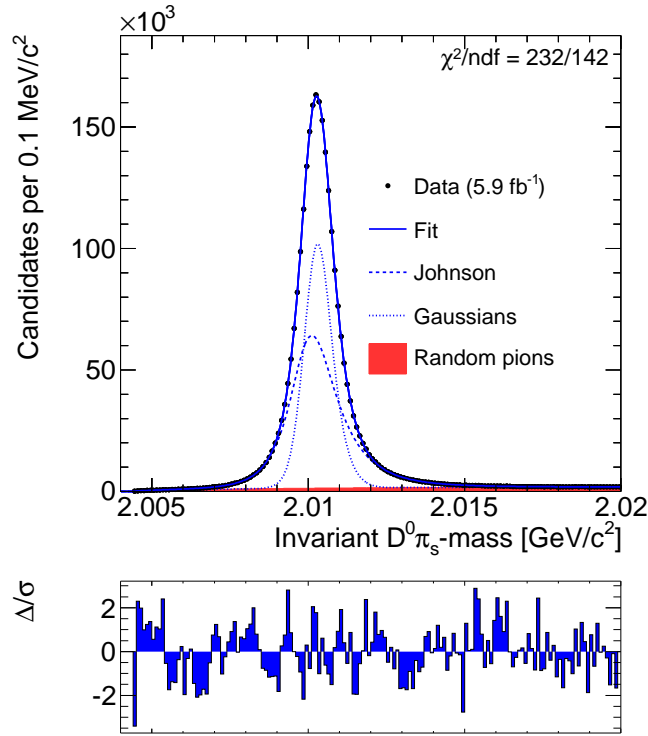


FIG. 6. Distribution of  $D^0\pi_s$  mass of tagged  $D^0 \rightarrow K^-\pi^+$  decays with fit results overlaid. The total fit projection (blue) is shown along with the double Gaussian bulk (dotted line), the Johnson tail (dashed line) and the background (full hatching).

582 and (b) show the projections of this simultaneous fit on the  $D^0\pi_s$  mass distribution, for  
 583 the tagged  $D^0 \rightarrow K^-\pi^+$  sample. Figures 7 (c) shows the projection on the asymmetry  
 584 distribution as a function of the  $D^0\pi_s$  mass. The asymmetry distribution is constructed by  
 585 evaluating bin-by-bin the difference and sum of the distributions in mass for charm ( $m_+$ )  
 586 and anti-charm ( $m_-$ ) decays to obtain  $A = (m_+ - m_-)/(m_+ + m_-)$ . The variation of the  
 587 asymmetry as a function of mass indicates whether backgrounds with asymmetries different  
 588 from the signal are present. As shown by the difference plots at the bottom of Fig. 7, the  
 589 fits correctly describe the asymmetry across the whole mass range.

590 We allowed independent  $\delta_J$  parameters in the charm and anti-charm samples because the  
 591  $D^0\pi_s$  mass distribution for  $D^{*+}$  candidates has slightly higher tails and a different width  
 592 than the corresponding distribution for  $D^{*-}$  candidates. The relative difference between the  
 593 resulting  $\delta_J$  values does not exceed 0.5%. However, by allowing the parameter  $\delta_J$  to vary  
 594 independently the  $\chi^2/\text{ndf}$  value improves from 414/306 to 385/304. We do not expect the

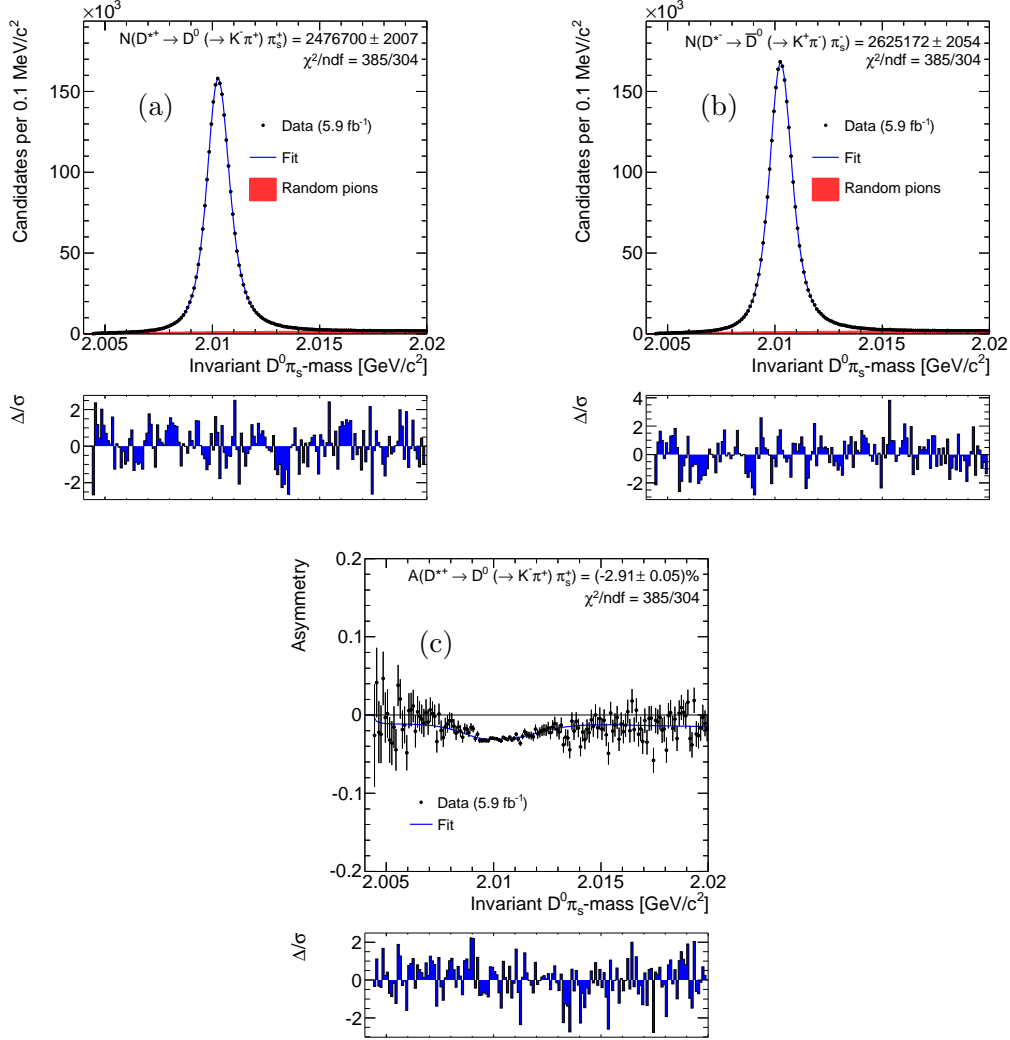


FIG. 7. Results of the combined fit of the tagged  $D^0 \rightarrow K^- \pi^+$  samples. Distribution of  $D^0 \pi_s$  mass for (a) charm, and (b) anti-charm decays, and (c) asymmetry as a function of the mass. Fit results are overlaid.

595 source of this difference to be asymmetric background because the difference is maximally  
 596 visible in the signal region, where the kinematic correlation between  $D^0 \pi_s$  mass and  $\pi_s$   
 597 transverse momentum is stronger. Indeed, small differences between  $D^{*+}$  and  $D^{*-}$  shapes  
 598 may be expected because the drift chamber has different resolutions for positive and nega-  
 599 tive low momentum particles. Independent  $\delta_J$  parameters provide a significantly improved  
 600 description of the asymmetry as a function of  $D^0 \pi_s$  mass in the signal region (Fig. 7 (c)). In  
 601 Sec. IX D we report a systematic uncertainty associated with this assumption. No significant  
 602 improvement in fit quality is observed when leaving other shape parameters free to

603 vary independently for  $D^{*+}$  and  $D^{*-}$  candidates.

The plots in Fig. 8 show the fit results for tagged  $D^0 \rightarrow \pi^+\pi^-$  and  $D^0 \rightarrow K^-K^+$  samples. In the  $D^0 \rightarrow K^+K^-$  fit we include an additional component from mis-reconstructed multibody decays. Because signal plus random pion shapes are fixed to those obtained by fitting the tagged  $K\pi$  sample (Fig. 7), the shape of this additional multibody component is conveniently extracted from the combined fit to data and is described by

$$\begin{aligned} \wp_{\text{mbd}}(m|\vec{\theta}_{\text{mbd}}) &= f_{\text{mbd}} J(m|m_{D^*} + \mu_{\text{mbd}}, \sigma_{\text{mbd}}, \delta_{\text{mbd}}, \gamma_{\text{mbd}}) \\ &\quad + (1 - f_{\text{mbd}}) \mathcal{B}(m|m_{D^0} + m_\pi, b_{\text{mbd}}, c_{\text{mbd}}). \end{aligned}$$

604 The total function used to fit the  $KK^*$  sample is then

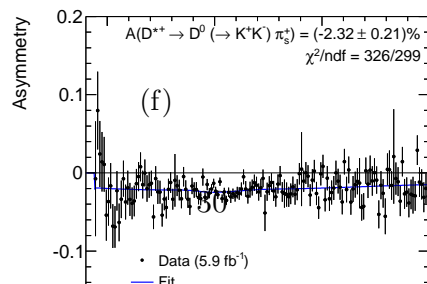
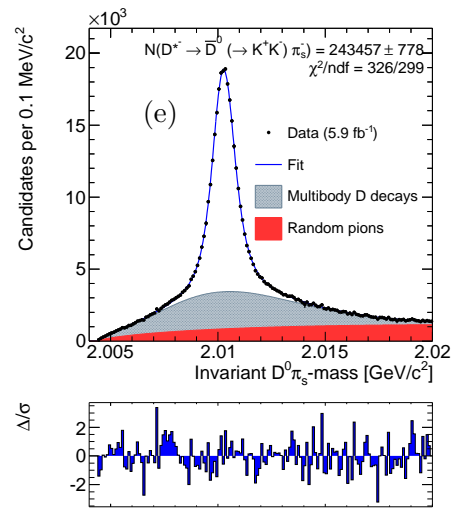
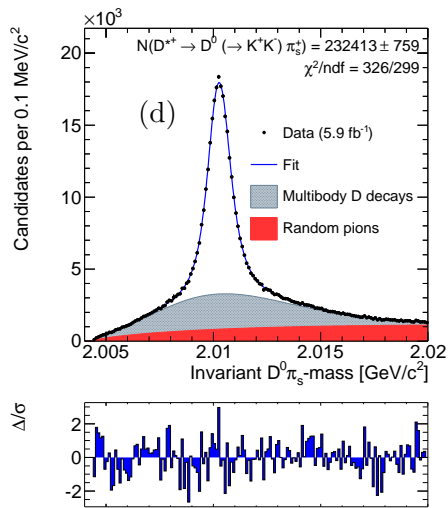
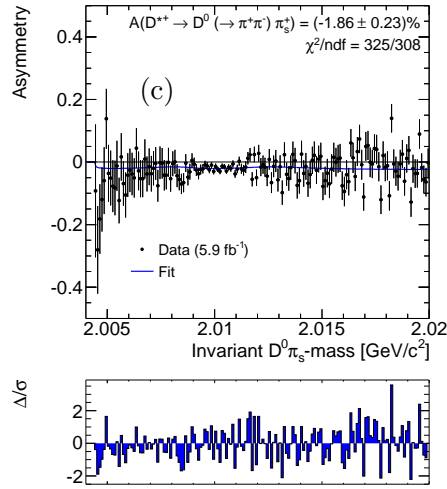
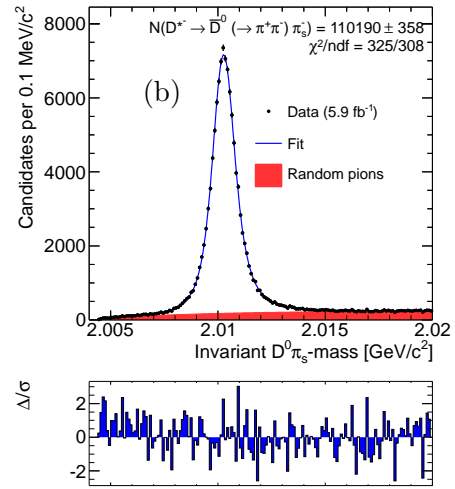
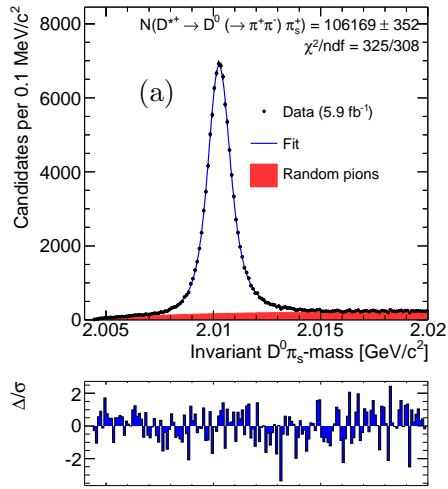
$$N_{\text{sig}} \wp_{\text{sig}}(m|\vec{\theta}_{\text{sig}}) + N_{\text{bkg}} \wp_{\text{bkg}}(m|\vec{\theta}_{\text{bkg}}) + N_{\text{mbd}} \wp_{\text{mbd}}(m|\vec{\theta}_{\text{mbd}}).$$

We observe the following asymmetries in the three tagged samples:

$$\begin{aligned} A(\pi\pi^*) &= (-1.86 \pm 0.23)\%, \\ A(KK^*) &= (-2.32 \pm 0.21)\%, \\ A(K\pi^*) &= (-2.910 \pm 0.049)\%. \end{aligned} \tag{7}$$

## 605 B. Fit of the untagged sample

606 In untagged  $K\pi$  decays no soft pion is associated with the neutral charm meson to form  
 607 a  $D^*$  candidate so there is no identification of its charm or anti-charm content. We infer  
 608 the flavor of the neutral charm meson on a statistical basis using the mass resolution of the  
 609 tracker and the quasi-flavor-specific nature of neutral charm decays into  $K\pi$  final states. The  
 610 role of mass resolution is evident in Fig. 5, which shows the distribution of  $K^-\pi^+$  mass as a  
 611 function of  $K^+\pi^-$  mass for the sample of untagged  $D^0 \rightarrow h^+h'^-$  decays. The cross-shaped  
 612 structure at the center of the plot is dominated by  $K\pi$  decays. In each mass projection  
 613 the narrow component of the structure is due to decays where the chosen  $K\pi$  assignment  
 614 is correct. The broader component is due to decays where the  $K\pi$  assignment is swapped.  
 615 In the momentum range of interest, the observed widths of these two components differ by  
 616 roughly an order of magnitude. Because of the CKM hierarchy of couplings, approximately  
 617 99.6% of neutral charm decays into a  $K^-\pi^+$  final state are from Cabibbo-favored decays



618 of  $D^0$  mesons, with only 0.4% from the doubly-suppressed decays of  $\overline{D}^0$  mesons, and vice  
619 versa for  $K^+\pi^-$  decays. Therefore, the narrow (broad) component in the  $K^-\pi^+$  projection  
620 is dominated by  $D^0$  ( $\overline{D}^0$ ) decays. Similarly, the narrow (broad) component in the  $K^+\pi^-$   
621 projection is dominated by  $\overline{D}^0$  ( $D^0$ ) decays.

622 We extract the asymmetry between charm and anti-charm decays in the untagged sample  
623 from a simultaneous binned fit of the  $K^+\pi^-$  and  $K^-\pi^+$  mass distributions in two independent  
624 subsamples. We randomly divide the untagged sample into two independent subsamples,  
625 equal in size, whose events were collected in the same data-taking period (“odd” and “even”  
626 sample). We arbitrarily choose to reconstruct the  $K^-\pi^+$  mass for candidates of the odd  
627 sample and the  $K^+\pi^-$  mass for candidates of the even sample. In the odd sample the  
628 decay  $D^0 \rightarrow K^-\pi^+$  is considered “right sign” (RS) because it is reconstructed with proper  
629 mass assignment. In the even sample it is considered a “wrong sign” (WS) decay, since it  
630 is reconstructed with swapped mass assignment. The opposite holds for the  $\overline{D}^0 \rightarrow K^+\pi^-$   
631 decay. The shapes used in the fit are the same for odd and even samples. The fit determines  
632 the number of  $D^0 \rightarrow K^-\pi^+$  (RS decays) from the odd sample and the number of  $\overline{D}^0 \rightarrow$   
633  $K^+\pi^-$  (RS decays) from the even sample thus determining the asymmetry. We split the  
634 total untagged sample in half to avoid the need to account for correlations. The reduction  
635 in statistical power has little practical effect since half of the untagged  $K\pi$  decays are still  
636 30 (67) times more abundant than the tagged  $K^+K^-$  ( $\pi^+\pi^-$ ) decays, and the corresponding  
637 statistical uncertainty gives a negligible contribution to the uncertainty of the final result.

The mass shapes used in the combined fit of the untagged sample are extracted from  
simulated events and adjusted by fitting the  $K\pi$  mass distribution in data. All functions  
described in the following are properly normalized when used in fits. The mass line shape  
of right-sign decays is parameterized using the following analytical expression:

$$\begin{aligned} \wp_{\text{RS}}(m|\vec{\theta}_{\text{RS}}) = & f_{\text{bulk}}[f_1\mathcal{G}(m|m_{D^0} + \delta_1, \sigma_1) \\ & + (1 - f_1)\mathcal{G}(m|m_{D^0} + \delta_2, \sigma_2)] \\ & + (1 - f_{\text{bulk}})\mathcal{T}(m|b, c, m_{D^0} + \delta_1), \end{aligned}$$

638 where

$$\mathcal{T}(m|b, c, \mu) = e^{b(m-\mu)}\text{Erfc}(c(m-\mu)),$$

with  $\text{Erfc}(x) = (2/\sqrt{\pi})\int_x^{+\infty} e^{-t^2} dt$ . We use the sum of two Gaussians to parameterize the  
bulk of the distribution. The function  $\mathcal{T}(m; b, c, \mu)$  describes the lower-mass tail due to

the soft photon emission. The parameter  $f_{\text{bulk}}$  is the relative contribution of the double Gaussian. The parameter  $f_1$  is the fraction of dominant Gaussian, relative to the sum of the two Gaussians. The parameters  $\delta_{1(2)}$  are possible shifts in mass from the known  $D^0$  mass [1]. Because the soft photon emission makes the mass distribution asymmetric, the means of the Gaussians cannot be assumed to be the same. Therefore  $m_{D^0}$  is fixed in the parametrization while  $\delta_{1(2)}$  are determined by the fit. The mass distribution of wrong-sign decays,  $\wp_{\text{WS}}(m; \vec{\theta}_{\text{WS}})$ , is parameterized using the same functional form used to model RS decays. The mass distribution of  $D^0 \rightarrow \pi^+\pi^-$  decays is modeled using the following functional form:

$$\begin{aligned} \wp_{\pi\pi}(m|\vec{\theta}_{\pi\pi}) = & f_{\text{bulk}}[f_1\mathcal{G}(m|m_0 + \delta_1, \sigma_1) + \\ & (1 - f_1)\mathcal{G}(m|m_0 + \delta_2, \sigma_2)] \\ & + f_{t1}\mathcal{T}(m|b_1, c_1, m_1) \\ & + (1 - f_{\text{bulk}} - f_{t1})\mathcal{T}(m|b_2, c_2, m_2). \end{aligned}$$

639 The bulk of the distribution is described by two Gaussians. Two tail functions  $\mathcal{T}(m; b, c, \mu)$   
640 are added for the low- and high-mass tails due to soft photon emission and incorrect mass  
641 assignment, respectively. The shifts in mass,  $\delta_{1(2)}$ , from the empirical value of the mass of  $\pi\pi$   
642 decays assigned the  $K\pi$  mass,  $m_0 = 1.96736 \text{ GeV}/c^2$ , are free to vary. The mass distributions  
643 of the partially reconstructed multibody charm decays and combinatorial background are  
644 modeled using decreasing exponential functions with coefficients  $b_{\text{mbd}}$  and  $b_{\text{comb}}$ , respectively.

The function used in the fit is then

$$\begin{aligned} & N_{\text{RS}}\wp_{\text{RS}}(m|\vec{\theta}_{\text{RS}}) + N_{\text{WS}}\wp_{\text{WS}}(m|\vec{\theta}_{\text{WS}}) \\ & + N_{\pi\pi}\wp_{\pi\pi}(m|\vec{\theta}_{\pi\pi}) + N_{\text{mbd}}\wp_{\text{mbd}}(m|b_{\text{mbd}}) \\ & + N_{\text{comb}}\wp_{\text{comb}}(m|b_{\text{comb}}). \end{aligned}$$

645 where  $N_{\text{RS}}$ ,  $N_{\text{WS}}$ ,  $N_{\pi\pi}$ ,  $N_{\text{mbd}}$ ,  $N_{\text{comb}}$  are the event yields for right-sign decays, wrong-sign  
646 decays,  $D^0 \rightarrow \pi^+\pi^-$  decays, partially reconstructed decays, and combinatorial background,  
647 respectively.

648 The mass is fit in the range  $1.8 < m < 2.4 \text{ GeV}/c^2$  to avoid the need for modeling most  
649 of the partially reconstructed charm meson decays. The ratio  $N_{\text{RS}}/N_{\text{mbd}}$  and the parameter  
650  $b_{\text{mbd}}$  are fixed from simulated inclusive  $D^0$  and  $D^+$  decays. The contamination from partially

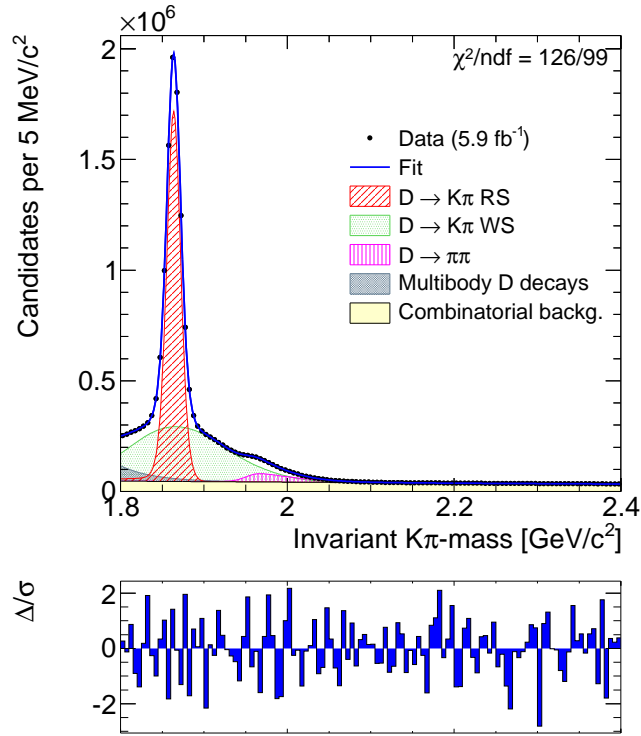


FIG. 9. Average ( $m$ ) of the distribution of  $K^+\pi^-$  mass in the even sample and  $K^-\pi^+$  mass in the odd sample with fit projections overlaid.

reconstructed  $D_s^+$  decays is negligible for masses greater than 1.8  $\text{GeV}/c^2$ . The result of the fit to the distribution averaged between odd and even samples is shown in Fig. 9. In this preliminary fit we let vary the number of events in each of the various components, the parameters of the two Gaussians describing the bulk of the  $D^0 \rightarrow h^+h^-$  distributions, and the slope of the combinatorial background  $b_{\text{comb}}$ . We assume that the small tails are described accurately enough by the simulation. This preliminary fit is used to extract all shape parameters that will be fixed in the subsequent combined fit for the asymmetry.

Odd and even samples are fitted simultaneously using the same shapes for each component to determine the asymmetry of RS decays. Because no asymmetry in  $D^0 \rightarrow \pi^+\pi^-$  decays and combinatorial background is expected by construction, we include the following constraints:  $N_{\pi\pi}^+ = N_{\pi\pi}^-$  and  $N_{\text{comb}}^+ = N_{\text{comb}}^-$ . The parameters  $N_{\text{RS}}^+$ ,  $N_{\text{RS}}^-$ ,  $N_{\text{WS}}^+$ ,  $N_{\text{WS}}^-$ ,  $N_{\text{mbd}}^+$  and  $N_{\text{mbd}}^-$  are determined by the fit independently in the even and odd samples. Figures 10 (a) and (b) show the fit projections for odd and even samples. Figure 10 (c) shows the projection of the simultaneous fit on the asymmetry as a function of the  $K\pi$  mass. The observed asymmetry

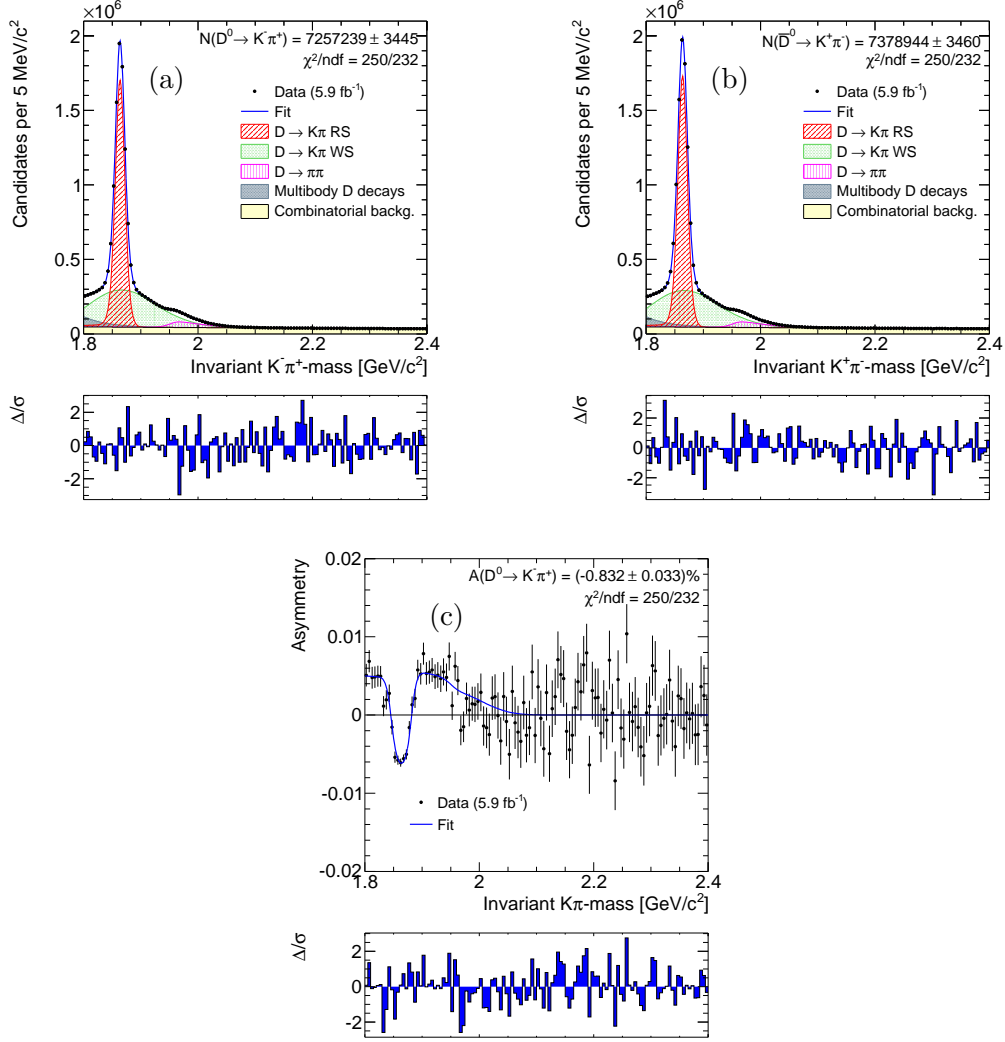


FIG. 10. Results of the combined fit of the untagged  $D^0 \rightarrow K^- \pi^+$  sample. Distribution of  $D^0 \pi_s$  mass for (a) charm, and (b) anti-charm decays, and (c) asymmetry as a function of the mass. Fit results are overlaid.

666 for the  $D^0 \rightarrow K^- \pi^+$  RS decays is

$$A(K\pi) = (-0.832 \pm 0.033)\%. \quad (8)$$

## 667 IX. SYSTEMATIC UNCERTAINTIES

668 The measurement strategy is designed to suppress systematic uncertainties. However,  
669 we consider a few residual sources that can impact the results: approximations in the sup-  
670 pression of detector-induced asymmetries; production asymmetries; contamination from sec-

671 onday  $D$  mesons; assumptions and approximations in fits, which include specific choice of  
672 analytic shapes, differences between distributions associated with charm and anti-charm  
673 decays, and contamination from unaccounted backgrounds; and, finally, assumptions and  
674 limitations of kinematic reweighting.

675 Most of the systematic uncertainties are evaluated by modifying the fit functions to  
676 include systematic variations and repeating the fits to data. The differences between results  
677 of modified fits and the central one are used as systematic uncertainties. This usually  
678 overestimates the observed size of systematic uncertainties, which include an additional  
679 statistical component. However, the additional uncertainty is negligible, given the size of the  
680 event samples involved. Sources of systematic uncertainty are detailed below. A summary  
681 of the most significant uncertainties is given in Table III.

#### 682 **A. Approximations in the suppression of detector-induced effects**

683 We check the reliability of the cancellation of all detector-induced asymmetries on sim-  
684 ulated samples as described in Appendix B. The analysis is repeated on several statistical  
685 ensembles in which we introduce known  $CP$ -violating asymmetries in the  $D^0 \rightarrow h^+ h^{(\prime)-}$   
686 decays and instrumental effects (asymmetric reconstruction efficiency for positive and neg-  
687 ative soft pions and kaons) dependent on a number of kinematic variables (e.g., transverse  
688 momentum). These studies constrain the size of residual instrumental effects that might not  
689 be fully cancelled by our method of linear subtraction of asymmetries. They also assess the  
690 impact of possible correlations between reconstruction efficiencies of  $D^0$  decay-products and  
691 the soft pion, which are assumed negligible in the analysis. We further check this assump-  
692 tion on data by searching for any variation of the observed asymmetry as a function of the  
693 proximity between the soft pion and the charm meson trajectories. No variation is found.

694 Using the results obtained with realistic values for the simulated effects, we assess a  
695  $\Delta A_{CP}(hh) = 0.009\%$  uncertainty. This corresponds to the maximum shift, increased by  
696 one standard deviation, observed in the results, for true  $CP$ -violating asymmetries in input  
697 ranging from  $-5\%$  to  $+5\%$ .

698 **B. Production asymmetries**

699 Charm production in high-energy  $p\bar{p}$  collisions is dominated by  $CP$ -conserving  $c\bar{c}$  produc-  
700 tion through the strong interaction. No production asymmetries are expected by integrating  
701 over the whole phase space. However, the CDF acceptance covers a limited region of the  
702 phase space, where  $CP$  conservation may not be exactly realized. Correlations with the  
703  $p\bar{p}$  initial state may induce pseudorapidity-dependent asymmetries between the number of  
704 produced charm and anti-charm (or positive- and negative-charged) mesons. These asym-  
705 metries are constrained by  $CP$  conservation to change sign for opposite values of  $\eta$ . The net  
706 effect is expected to vanish if the pseudorapidity distribution of the sample is symmetric.

707 To set an upper limit to the possible effect of small residual  $\eta$  asymmetries of the samples  
708 used in this analysis, we repeat the fits enforcing a perfect  $\eta$  symmetry by reweighting.  
709 We observe variations of  $\Delta A_{CP}(KK) = 0.03\%$  and  $\Delta A_{CP}(\pi\pi) = 0.04\%$  between the fit  
710 results obtained with and without re-weighting. We take these small differences as an  
711 estimate of the size of possible residual effects. The cancellation of production asymmetries  
712 achieved in  $p\bar{p}$  collisions (an initial  $CP$ -symmetric state) recorded with a polar-symmetric  
713 detector provide a significant advantage in high-precision  $CP$ -violation measurements over  
714 experiments conducted in  $pp$  collisions.

715 **C. Contamination of  $D$  mesons from  $B$  decays**

716 A contamination of charm mesons produced in  $b$ -hadron decays could bias the results.  
717 Violation of  $CP$  symmetry in  $b$ -hadron decays may result in asymmetric production of  
718 charm and anti-charm mesons. This may be large for a single exclusive mode, but the  
719 effect is expected to vanish for inclusive  $B \rightarrow D^0 X$  decays [27]. However, we use the impact  
720 parameter distribution of  $D^0$  mesons to statistically separate primary and secondary mesons  
721 and assign a systematic uncertainty. Here, by “secondary” we mean any  $D^0$  originating from  
722 the decay of any  $b$  hadron regardless of the particular decay chain involved. In particular  
723 we do not distinguish whether the  $D^0$  meson is coming from a  $D^{*\pm}$  or not.

724 If  $f_B$  is the fraction of secondary  $D^0$  mesons in a given sample, the corresponding observed  
725 asymmetry  $A$  can be written as a linear combination of the asymmetries for primary and

726 secondary  $D^0$  mesons:

$$A = f_B A(D^0 \text{ secondary}) + (1 - f_B) A(D^0 \text{ primary}). \quad (9)$$

727 The asymmetry observed for secondary  $D^0$  mesons can be expressed, to first order, as the  
 728 sum of the asymmetry you would observe for a primary  $D^0$  sample, plus a possible  $CP$ -  
 729 violating asymmetry in inclusive  $B \rightarrow D^0 X$  decays,

$$A(D^0 \text{ sec.}) = A_{CP}(B \rightarrow D^0 X) + A(D^0 \text{ prim.}). \quad (10)$$

730 Hence, combining Eq. (9) and Eq. (10), the asymmetry observed in each sample is given by

$$A = f_B A_{CP}(B \rightarrow D^0 X) + A(D^0 \text{ primary}). \quad (11)$$

731 Because the fraction of secondary  $D^0$  mesons is independent of their decay mode, we assume  
 732  $f_B(\pi\pi^*) = f_B(KK^*) = f_B(K\pi^*)$ . The contribution of  $CP$  violation in  $b$ -hadron decays to  
 733 the final asymmetries is written as

$$A(hh) = f_B(K\pi) A_{CP}(B \rightarrow D^0 X) + A_{CP}(D^0 \rightarrow hh), \quad (12)$$

734 where  $f_B$  is estimated in the untagged  $K^-\pi^+$  sample because the two terms arising from  
 735 the tagged components cancel in the subtraction provided by Eq. (6). In this analysis, the  
 737 contamination from secondary  $D^0$  decays is reduced by requiring the impact parameter of  
 738 the  $D^0$  candidate,  $d_0(D^0)$ , not to exceed  $100 \mu\text{m}$ . The fraction  $f_B$  of residual  $D^0$  mesons  
 739 originating from  $B$  decays has been determined by fitting the distribution of the impact  
 740 parameter of untagged  $D^0 \rightarrow K^-\pi^+$  decays selected within  $\pm 24 \text{ MeV}/c^2$  of the known  $D^0$   
 741 mass [1]. We use two Gaussian distributions to model the narrow peak from primary  $D^0$   
 742 mesons and a binned histogram, extracted from a simulated sample of inclusive  $B \rightarrow D^0 X$   
 743 decays, to model the secondary component. Figure 11 shows the data with the fit projection  
 744 overlaid. A residual contamination of 16.6% of  $B \rightarrow D^0 X$  decays with impact parameter  
 745 lower than  $100 \mu\text{m}$  is estimated. To constrain the size of the effect from  $A_{CP}(B \rightarrow D^0 X)$   
 746 we repeat the analysis inverting the impact parameter selection, namely requiring  $d_0(D^0) >$   
 747  $100 \mu\text{m}$ . This selects an almost pure sample of  $D^0 \rightarrow K^-\pi^+$  decays from  $B$  decays ( $f_B = 1$ ).  
 748 We reconstruct about 900 000 decays with an asymmetry,  $A(K\pi) = (-0.647 \pm 0.172)\%$ ,  
 749 consistent with  $(-0.832 \pm 0.033)\%$ , the value used in our measurement. Using Eq. (10)

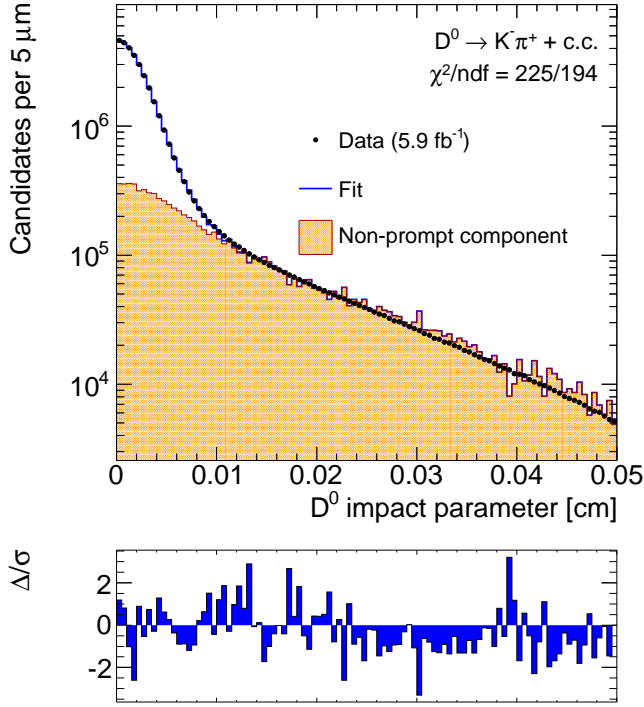


FIG. 11. Impact parameter distribution of  $D^0$  candidates in the  $D^0 \rightarrow K^- \pi^+$  signal region. Top plot with data and fit projections overlaid uses a logarithmic scale vertically. Bottom plot shows fractional difference between data and the fit on a linear scale.

750 we write the difference between the above asymmetry and the asymmetry observed in the  
751 central analysis (Eq. (12)),  $A(d_0 > 100 \mu\text{m}) - A(d_0 < 100 \mu\text{m})$ , as

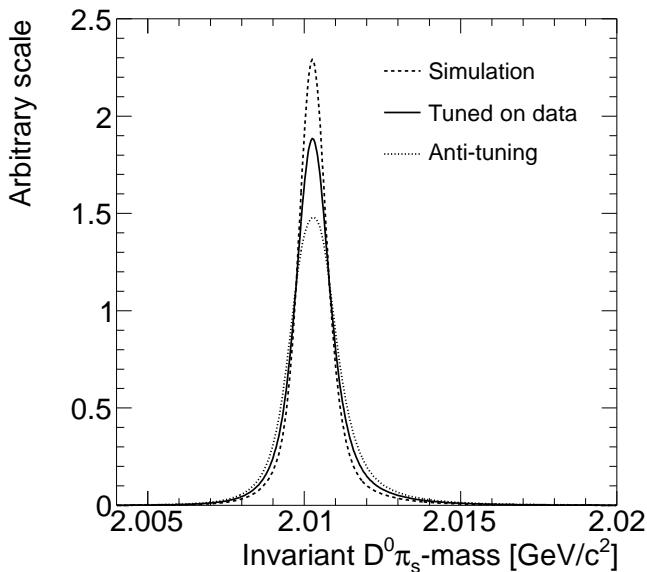
$$(1 - f_B)A_{CP}(B \rightarrow D^0 X) = (-0.18 \pm 0.17)\%. \quad (13)$$

752 Using  $f_B = 16.6\%$  we obtain  $A_{CP}(B \rightarrow D^0 X) = (-0.21 \pm 0.20)\%$  showing that no evidence  
753 for a bias induced by secondary  $D^0$  mesons is present. Based on Eq. (12), we assign a  
754 conservative systematic uncertainty evaluated as  $f_B A_{CP}(B \rightarrow DX) = f_B/(1 - f_B)\Delta =$   
755  $0.034\%$ , where  $f_B$  equals  $16.6\%$  and  $\Delta$  corresponds to the  $0.17\%$  standard deviation of the  
756 difference in Eq. (13).

757 **D. Assumptions in the fits of tagged samples**

758 *1. Shapes of fit functions*

759 The mass shape extracted from simulation has been adjusted using data for a more  
 760 accurate description of the observed signal shape. A systematic uncertainty is associated  
 761 with the finite accuracy of this tuning and covers the effect of possible mis-modeling of the  
 762 shapes of the fit components.



763

764 FIG. 12. Shape of  $D^0\pi_s$  mass as extracted from simulation without tuning, with data tuning and  
 765 with anti-data tuning.

766 Figure 12 shows a comparison between the shape extracted from the simulation and the  
 767 templates used in the fit after the tuning. It also shows an additional template, named  
 768 “anti-tuned”, where the corrections that adjust the simulation to data have been inverted.  
 769 If  $f(m)$  is the template tuned on data, and  $g(m)$  is the template extracted from the sim-  
 770 ulation, the anti-tuned template is constructed as  $h(m) = 2f(m) - g(m)$ . We repeat the  
 771 measurement using the templates extracted from the simulation without any tuning, and  
 772 those corresponding to the anti-tuning. The maximum variations from the central fit results,  
 773  $\Delta A_{CP}(\pi^+\pi^-) = 0.009\%$  and  $\Delta A_{CP}(K^+K^-) = 0.058\%$ , are assigned as systematic uncertain-  
 774 ties. The larger effect observed in the  $D^0 \rightarrow K^+K^-$  case comes from the additional degrees

775 of freedom introduced in the fit by the multibody-decays component.

776 In addition, we perform a cross-check of the shape used for the background of real  $D^0$   
777 mesons associated with random tracks. In the analysis, the shape parameters of  $D^0 \rightarrow h^+h^-$   
778 fits are constrained to the values obtained in the higher-statistics tagged  $D^0 \rightarrow K^-\pi^+$   
779 sample. If the parameters are left floating in the fit, only a negligible variation on the final  
780 result ( $< 0.003\%$ ) is observed.

## 781 2. Charge-dependent mass distributions

782 We observe small differences between distributions of  $D^0\pi_s$  mass for positive and negative  
783  $D^*$  candidates. These are ascribed to possible differences in tracking resolutions between  
784 low-momentum positive and negative particles. Such differences may impact our results  
785 at first order and would not be corrected by our subtraction method. To determine a  
786 systematic uncertainty, we repeat the fit in several configurations where various combinations  
787 of signal and background parameters are independently determined for positive and negative  
788  $D^*$  candidates. The largest effects are observed by leaving the background shapes to vary  
789 independently and constraining the parameter  $\delta_J$  of the Johnson function to be the same [25].  
790 The values of the shape parameters in  $D^0 \rightarrow h^+h^-$  fits are always fixed to the ones obtained  
791 from the  $D^0 \rightarrow K^-\pi^+$  sample. The maximum variations with respect to the central fits,  
792  $\Delta A_{CP}(\pi^+\pi^-) = 0.088\%$  and  $\Delta A_{CP}(K^+K^-) = 0.027\%$ , are used as systematic uncertainties.

## 793 3. Asymmetries from residual backgrounds

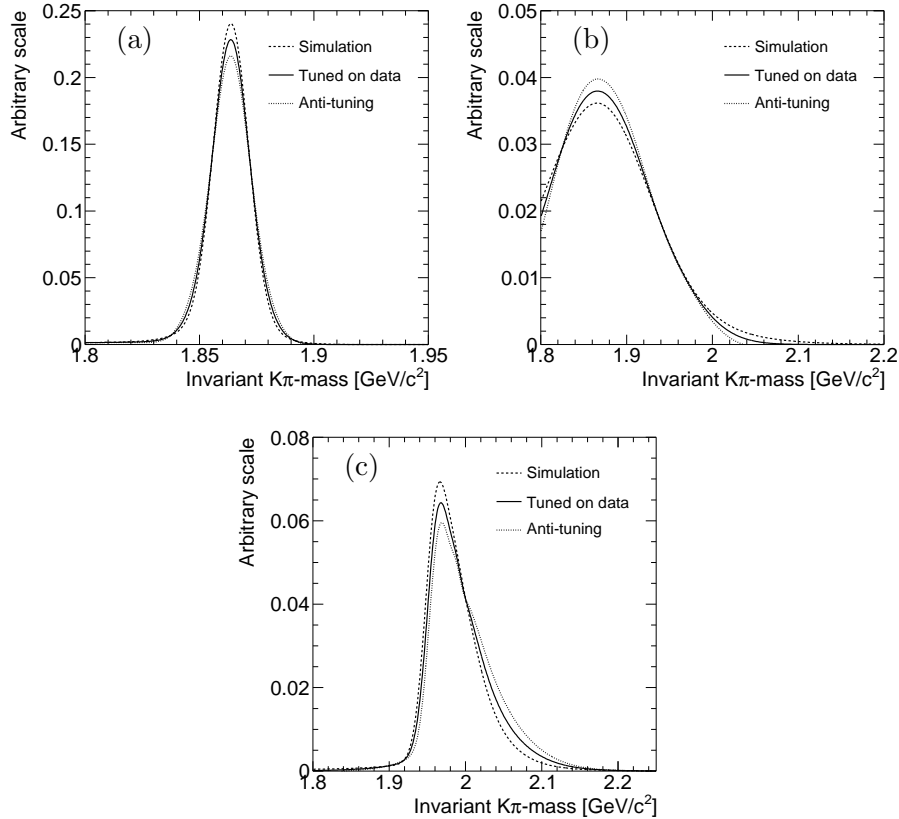
794 A further source of systematic uncertainty is the approximations used in the subtraction  
795 of physics backgrounds. In the  $K^+K^-$  sample we fit any residual background contribution,  
796 hence this uncertainty is absorbed in the statistical one. However, in the  $\pi^+\pi^-$  and  $K^-\pi^+$   
797 cases we assume the residual backgrounds to be negligible. Using simulation we estimate that  
798 a 0.22% and 0.77% contamination from physics backgrounds enters the  $\pm 24 \text{ MeV}/c^2$   $\pi^+\pi^-$   
799 and  $K^-\pi^+$  signal range, respectively. The contamination in the  $\pi^+\pi^-$  sample is dominated  
800 by the high mass tail of the  $D^0 \rightarrow K^-\pi^+$  signal. The asymmetry of this contamination is  
801 determined from a fit of the tagged  $K^-\pi^+$  sample. The contamination of the  $K^-\pi^+$  sample  
802 is dominated by the tail from partially reconstructed  $D^0$  decays. The fit of the tagged

803  $K^+K^-$  sample provides an estimate of the asymmetry of this contamination. In both cases  
 804 we assign a systematic uncertainty that is the product of the contaminating fraction times  
 805 the additional asymmetry of the contaminant. This yields a maximum effect of 0.005% on  
 806 the measured asymmetries for both  $D^0 \rightarrow \pi^+\pi^-$  and  $D^0 \rightarrow K^+K^-$  cases.

## 807 E. Assumptions in the fits of untagged samples

### 808 1. Shapes of fit functions

809 We follow the same strategy used for the tagged case to assign the systematic uncertainty  
 810 associated with possible mis-modeling of the shapes in fits of the untagged sample.



811  
 812  
 813 FIG. 13. Shapes of  $K^\pm\pi^\mp$  mass from simulation without tuning, with data tuning, and with  
 814 anti-data tuning for (a) right-sign and (b) wrong-sign  $K^\pm\pi^\mp$  decays, and for (c)  $\pi^+\pi^-$  decays.

815 Figure 13 shows the comparison between templates extracted from the simulation without  
 816 any tuning, those tuned to data (and used in the central fit), and the anti-tuned ones. We

817 repeat the fit using the templates from simulation and the anti-tuned ones. The maximum  
818 variation from the central fit,  $\Delta A(K\pi) = 0.005\%$ , is used as the systematic uncertainty.

## 819 2. Charge-dependent mass distributions

820 In the untagged case we expect the mass shapes of all components to be the same for  
821 charm and anti-charm samples. However, we repeat the simultaneous fit under different  
822 assumptions to assign the systematic uncertainty associated with possible residual differ-  
823 ences. The parameters of the Gaussian distributions used to model the bulk of the mass  
824 distributions are left free to vary independently for the charm and anti-charm samples, and  
825 separately for the right-sign, wrong-sign, and  $D \rightarrow \pi^+\pi^-$  components. We assume no dif-  
826 ference between mass distributions of combinatorial background and partially reconstructed  
827 decays. The differences between estimated shape parameters in charm and anti-charm sam-  
828 ples do not exceed  $3\sigma$ , showing compatibility between the shapes. A systematic uncertainty  
829 of  $0.044\%$  is obtained by summing in quadrature the shifts from the central values of the  
830 estimated asymmetries in the three different cases.

## 831 3. Asymmetries from residual physics backgrounds

832 In the measurement of the asymmetry of Cabibbo-favored  $D^0 \rightarrow K^-\pi^+$  decays, we  
833 neglect the contribution from the small, but irreducible, component of doubly-Cabibbo-  
834 suppressed (DCS)  $D^0 \rightarrow K^+\pi^-$  decays. Large  $CP$  violation in DCS decays may bias the  
835 charge asymmetry we attribute to  $D^0 \rightarrow K^-\pi^+$  decays. We assign a systematic uncertainty  
836 corresponding to  $f_{DCS}A_{CP}(D^0 \rightarrow K^+\pi^-) = f_{DCS}\Delta = 0.013\%$ , where  $f_{DCS} = 0.39\%$  is the  
837 known [1] fraction of DCS decays with respect to Cabibbo-favored decays and  $\Delta = 2.2\%$   
838 corresponds to one standard deviation of the current measured limit on the  $CP$ -violating  
839 asymmetry  $A_{CP}(D^0 \rightarrow K^+\pi^-)$  as reported in Ref. [1].

840 In the central fit for the untagged  $D^0 \rightarrow K^-\pi^+$  sample, no asymmetry in  $D^0 \rightarrow \pi^+\pi^-$  de-  
841 cays or combinatorial background is included, as expected by the way the untagged sample  
842 is defined. We confirm the validity of this choice by fitting the asymmetry with indepen-  
843 dent parameters for these two shapes in the charm and anti-charm samples. The result  
844 corresponds to a  $\Delta A(K\pi) = 0.011\%$  variation from the central fit.

## 845 **F. Limitations of kinematic reweighting**

846 The tagged event samples are reweighted after subtracting the background, sampled in  
847 signal mass sidebands. We constrain the size of possible residual systematic uncertainties  
848 by repeating the fit of tagged  $D^0 \rightarrow h^+h^-$  after a reweighting without any sideband sub-  
849 traction. The variation in observed asymmetries is found to be negligible with respect to  
850 other systematic uncertainties.

851 In reweighting the untagged sample we do not subtract the background. The signal  
852 distributions are extracted by selecting a mass region corresponding approximately to a  
853 cross-shaped window of  $\pm 3\sigma$  in the two-dimensional space  $(M(K^+\pi^-), M(K^-\pi^+))$ . To  
854 assign a systematic uncertainty we extract the signal distributions and reweight the data  
855 using a smaller cross-shaped region of  $\pm 2\sigma$  (i.e. within  $16 \text{ MeV}/c^2$  from the nominal  $D^0$   
856 mass). The background contamination decreases from 6% to 4%. We repeat the analysis  
857 and find  $A(K\pi) = (-0.831 \pm 0.033)\%$  corresponding to a variation from the central fit of  
858  $< 0.001\%$ , thus negligible with respect to other systematic uncertainties.

## 859 **G. Total systematic uncertainty**

860 Table III summarizes the most significant systematic uncertainties considered in the mea-  
861 surement. Assuming them independent and summing in quadrature, we obtain a total sys-  
862 tematic uncertainty of 0.11% on the observed  $CP$ -violating asymmetry of  $D^0 \rightarrow \pi^+\pi^-$  de-  
863 cays and 0.09% in  $D^0 \rightarrow K^+K^-$  decays. Their sizes are approximately half of the statistical  
864 uncertainties.

## 865 **X. FINAL RESULT**

Using the observed asymmetries from Eqs. (7) and (8) in the relationships of Eq. (5), we determine the time-integrated  $CP$ -violating asymmetries in  $D^0 \rightarrow \pi^+\pi^-$  and  $D^0 \rightarrow K^+K^-$  decays to be

$$A_{CP}(\pi^+\pi^-) = (+0.22 \pm 0.24 \text{ (stat)} \pm 0.11 \text{ (syst)})\%$$
$$A_{CP}(K^+K^-) = (-0.24 \pm 0.22 \text{ (stat)} \pm 0.09 \text{ (syst)})\%,$$

TABLE III. Summary of most significant systematic uncertainties. The uncertainties reported for the last three sources result from the sum in quadrature of the contributions in the tagged and untagged fits.

Source	$A_{CP}(\pi^+\pi^-)$ [%]	$A_{CP}(K^+K^-)$ [%]
Approximations in the suppression of detector-induced effects	0.009	0.009
Production asymmetries	0.040	0.030
Contamination of secondary $D$ mesons	0.034	0.034
Shapes assumed in fits	0.010	0.058
Charge-dependent mass distributions	0.098	0.052
Asymmetries from residual backgrounds	0.014	0.014
Limitations of sample reweighting	< 0.001	< 0.001
Total	0.113	0.092

866 corresponding to  $CP$  conservation in the time-evolution of these decays. These are the most  
 867 precise determinations of these quantities to date, and significantly improve the world's  
 868 average values. The results are also in agreement with theory predictions [28, 29].

869 A useful comparison with results from other experiments is achieved by expressing the  
 870 observed asymmetry as a linear combination (Eq. (4)) of a direct component,  $A_{CP}^{\text{dir}}$ , and an  
 871 indirect component,  $A_{CP}^{\text{ind}}$ , through a coefficient that is the mean proper decay time of charm  
 872 mesons in the data sample. The direct component corresponds to a difference in width  
 873 between charm and anti-charm decays into the same final state. The indirect component  
 874 is due to the probability for a charm meson to oscillate into an anti-charm meson being  
 875 different from the probability for an anti-charm meson to oscillate into a charm meson.

877 The decay time of each  $D^0$  meson,  $t$ , is determined as

$$t = \frac{L_{xy}}{c(\beta\gamma)_T} = L_{xy} \frac{m_{D^0}}{c p_T},$$

878 where  $(\beta\gamma)_T = p_T/m_{D^0}$  is the transverse Lorentz factor. This is an unbiased estimate of  
 879 the actual decay time only for primary charmed mesons. For secondary charm, the decay  
 880 time of the parent  $B$  meson should be subtracted. The mean decay times of our signals are  
 881 determined from a fit to the proper decay time distribution of sideband-subtracted tagged  
 882 decays (Fig. 14). The fit includes components for primary and secondary  $D$  mesons, whose

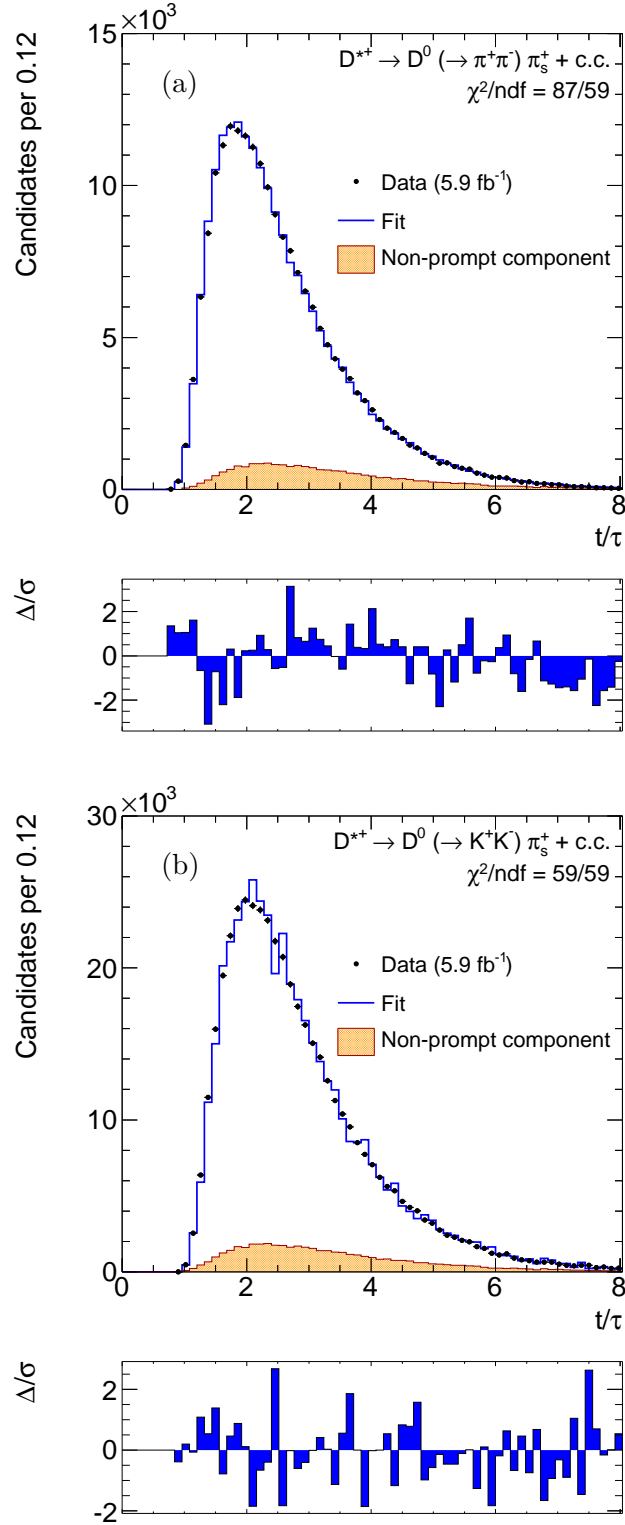


FIG. 14. Distribution of proper decay time (in units of  $D^0$  lifetime) for sideband-subtracted tagged (a)  $D^0 \rightarrow \pi^+\pi^-$  and (b)  $D^0 \rightarrow K^+K^-$  data. Fit results are overlaid including the component from secondary charmed mesons (red).

883 shapes are modeled from simulation. The simulation is used to extract the information on  
 884 the mean decay time of secondary charmed decays, using the known true decay time. The  
 885 proportions between primary and secondary are also determined from this fit and are con-  
 886 sistent with results of the fit to the  $D^0$  impact parameter in data (Sec. IX C). We determine  
 887 a mean decay time of  $2.40 \pm 0.03$  and  $2.65 \pm 0.03$ , in units of  $D^0$  lifetime, for  $D^0 \rightarrow \pi^+\pi^-$   
 888 and  $D^0 \rightarrow K^+K^-$  decays, respectively. The uncertainty is the sum in quadrature of sta-  
 889 tistical and systematic contributions. The small difference in the two samples is caused by  
 890 the slightly different kinematic distributions of the two decays, which impacts their trigger  
 891 acceptance.

892 Each of our measurements defines a band in the  $(A_{CP}^{\text{ind}}, A_{CP}^{\text{dir}})$  plane with slope  $-\langle t \rangle / \tau$   
 893 (Eq. (4)). The same holds for *BABAR* and Belle measurements, with slope  $-1$  [9, 10], due to  
 894 unbiased acceptance in decay time. The results of this measurement and the most recent *B-*  
 895 factories' results are shown in Fig. 15, which displays their relationship. The bands represent  
 896  $\pm 1\sigma$  uncertainties and show that all measurements are compatible with *CP* conservation (ori-  
 897 gin in the two-dimensional plane). The results of the three experiments can be combined as-  
 898 suming Gaussian uncertainties. We construct combined confidence regions in the  $(A_{CP}^{\text{ind}}, A_{CP}^{\text{dir}})$   
 899 plane, denoted with 68% and 95% confidence level ellipses. The corresponding values for the  
 900 asymmetries are  $A_{CP}^{\text{dir}}(D^0 \rightarrow \pi^+\pi^-) = (0.04 \pm 0.69)\%$ ,  $A_{CP}^{\text{ind}}(D^0 \rightarrow \pi^+\pi^-) = (0.08 \pm 0.34)\%$ ,  
 901  $A_{CP}^{\text{dir}}(D^0 \rightarrow K^+K^-) = (-0.24 \pm 0.41)\%$ , and  $A_{CP}^{\text{ind}}(D^0 \rightarrow K^+K^-) = (0.00 \pm 0.20)\%$ , in which  
 902 the uncertainties represent one-dimensional 68% confidence level intervals.

### 903 A. CP violation from mixing only

Assuming negligible direct *CP* violation in both decay modes, the observed asymmetry  
 is only due to mixing,  $A_{CP}(h^+h^-) \approx A_{CP}^{\text{ind}} \langle t \rangle / \tau$ , yielding

$$A_{CP}^{\text{ind}}(\pi^+\pi^-) = (+0.09 \pm 0.10 \text{ (stat)} \pm 0.05 \text{ (syst)})\%$$

$$A_{CP}^{\text{ind}}(K^+K^-) = (-0.09 \pm 0.08 \text{ (stat)} \pm 0.03 \text{ (syst)})\%.$$

904 Assuming that no large weak phases from non-SM contributions appear in the decay am-  
 905 plitudes,  $A_{CP}^{\text{ind}}$  is independent of the final state. Therefore the two measurements can be  
 906 averaged, assuming correlated systematic uncertainties, to obtain a precise determination of

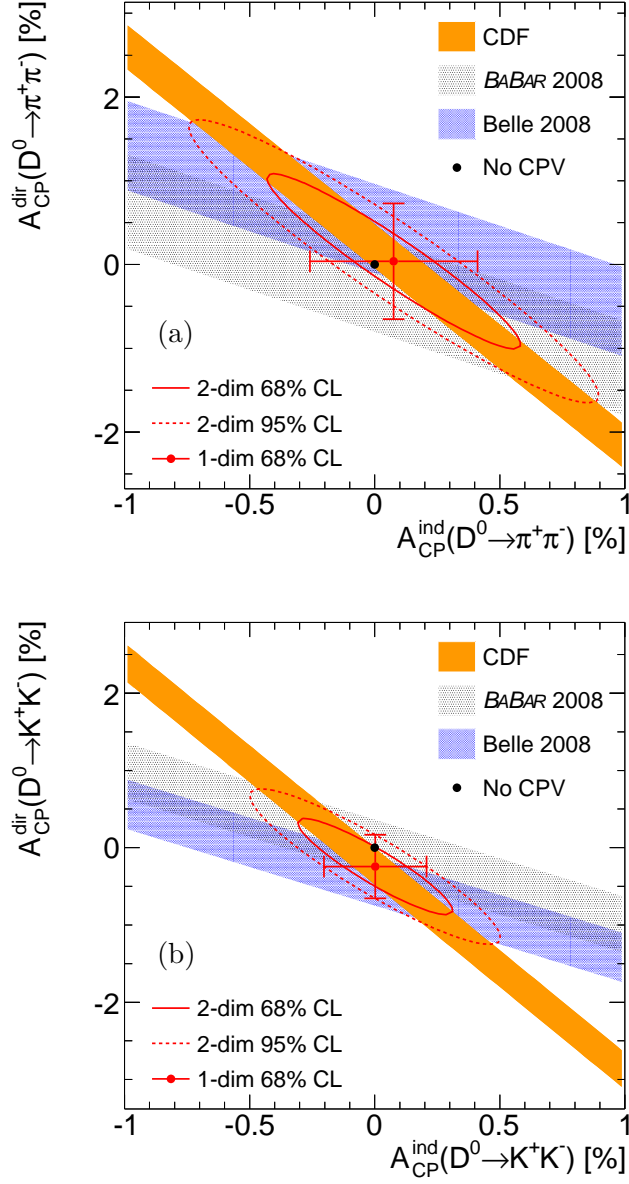


FIG. 15. Comparison of the present results with Belle and *BABAR* measurements of time-integrated  $CP$ -violating asymmetry in (a)  $D^0 \rightarrow \pi^+\pi^-$  and (b)  $D^0 \rightarrow K^+K^-$  decays displayed in the  $(A_{CP}^{\text{ind}}, A_{CP}^{\text{dir}})$  plane. The point with error bars denotes the central value of the combination of the three measurements with one-dimensional 68% confidence level uncertainties.

907  $CP$  violation in charm mixing:

$$A_{CP}^{\text{ind}}(D^0) = (-0.01 \pm 0.06 \text{ (stat)} \pm 0.04 \text{ (syst)})\%.$$

908 This corresponds to the following upper limits on  $CP$  violation in charm mixing:

$$|A_{CP}^{\text{ind}}(D^0)| < 0.13 \text{ (0.16)\% at the 90 (95)\% C.L.}$$

909 The bias toward longer-lived decays of the CDF sample offers a significant advantage over  
910  $B$ -factories in sensitivity to the time-dependent component, as shown in Figs. 16 (a), (c).

### 911 B. Direct $CP$ violation only

912 Assuming that  $CP$  symmetry is conserved in charm mixing, our results are readily com-  
913 parable to measurements obtained at  $B$ -factories;  $A_{CP}(\pi^+\pi^-) = (0.43 \pm 0.52 \text{ (stat)} \pm$   
914  $0.12 \text{ (syst)})\%$  and  $A_{CP}(K^+K^-) = (-0.43 \pm 0.30 \text{ (stat)} \pm 0.11 \text{ (syst)})\%$  from Belle, and  
915  $A_{CP}(\pi^+\pi^-) = (-0.24 \pm 0.52 \text{ (stat)} \pm 0.22 \text{ (syst)})\%$  and  $A_{CP}(K^+K^-) = (0.00 \pm 0.34 \text{ (stat)} \pm$   
916  $0.13 \text{ (syst)})\%$  from  $B\bar{A}R$  (Figs. 16 (b)-(d)). The CDF result is the world's most precise.

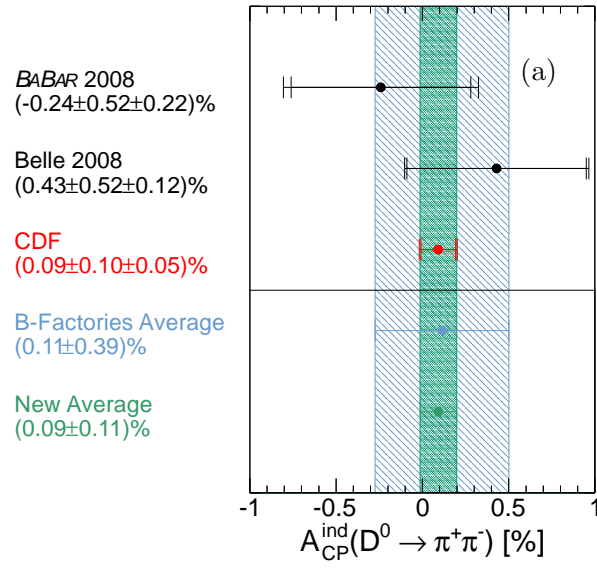
### 917 C. Difference of asymmetries

A useful comparison with theory predictions is achieved by calculating the difference be-  
tween the asymmetries observed in the  $D^0 \rightarrow K^+K^-$  and  $D^0 \rightarrow \pi^+\pi^-$  decays ( $\Delta A_{CP}$ ). Since  
the difference in decay-time acceptance is small,  $\Delta\langle t \rangle/\tau = 0.26 \pm 0.01$ , most of the indirect  
 $CP$ -violating asymmetry cancels in the subtraction, assuming that no large  $CP$ -violating  
phases from non-SM contributions enter the decay amplitudes. Hence  $\Delta A_{CP}$  approximates  
the difference in direct  $CP$ -violating asymmetries of the two decays. Using the observed  
asymmetries from Eq. (7), we determine

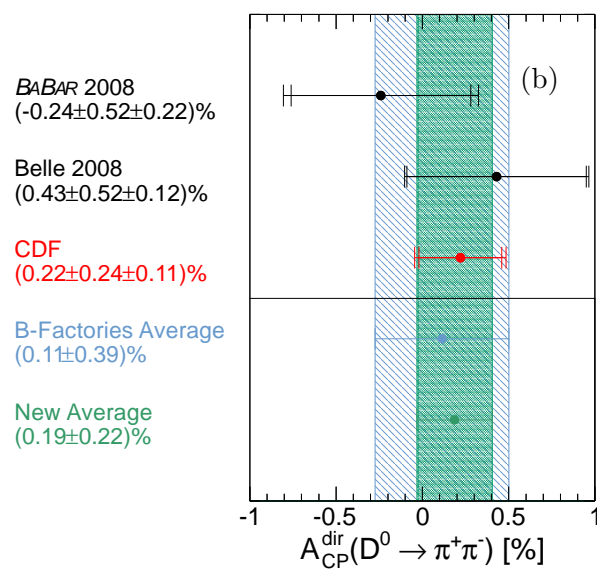
$$\begin{aligned} \Delta A_{CP} &= A_{CP}(K^+K^-) - A_{CP}(\pi^+\pi^-) \\ &= \Delta A_{CP}^{\text{dir}} + A_{CP}^{\text{ind}}\Delta\langle t \rangle/\tau \\ &= A(KK^*) - A(\pi\pi^*) \\ &= (-0.46 \pm 0.31 \text{ (stat)} \pm 0.12 \text{ (syst)})\%. \end{aligned}$$

918 The systematic uncertainty is dominated by the 0.12% uncertainty from the shapes as-  
919 sumed in the mass fits, and their possible dependence on the charge of the  $D^*$  meson. This  
920 is determined by combining the difference of shifts observed in Secs. IX D 1 and IX D 2 in-  
921 cluding correlations:  $(0.058 - 0.009)\% = 0.049\%$  and  $(-0.027 - 0.088)\% = 0.115\%$ . Smaller

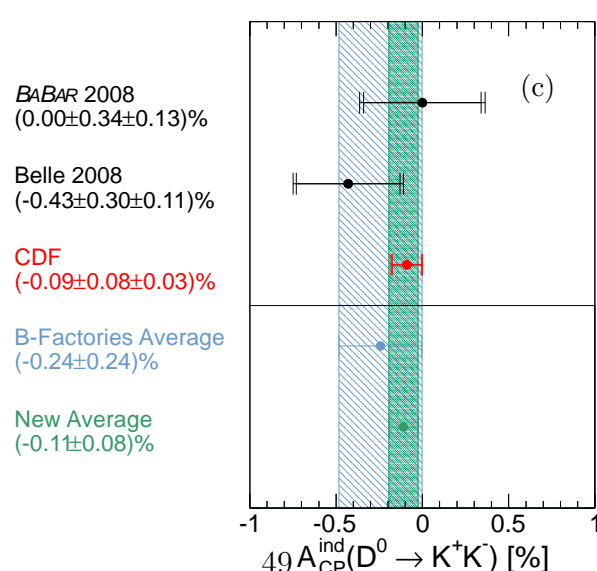
No direct CPV



No indirect CPV



No direct CPV



No indirect CPV

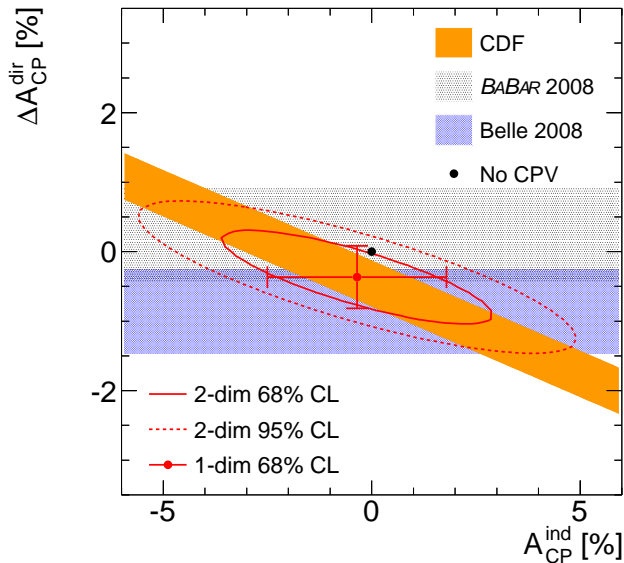


FIG. 17. Difference between direct  $CP$ -violating asymmetries in the  $K^+K^-$  and  $\pi^+\pi^-$  final states as a function of the indirect asymmetry. Belle and  $BABAR$  measurements are also reported for comparison. The point with error bars denotes the central value of the combination of the three measurements with one-dimensional 68% confidence level uncertainties.

922 contributions include a 0.009% from the finite precision associated to the suppression of  
 923 detector-induced effects (Sec. IX A), and a 0.005% due to the 0.22% background we ignore  
 924 under the  $D^0 \rightarrow \pi^+\pi^-$  signal (Sec. IX D 3). The effects of production asymmetries and  
 925 contamination from secondary charm decays cancel in the difference.

926 We see no evidence of a difference in  $CP$  violation between  $D^0 \rightarrow K^+K^-$  and  $D^0 \rightarrow \pi^+\pi^-$   
 927 decays. Figure 17 shows the difference in direct asymmetry ( $\Delta A_{CP}^{\text{dir}}$ ) as a function of the  
 928 indirect asymmetry compared with experimental results from  $BABAR$  and Belle [9, 10].  
 929 The bands represent  $\pm 1\sigma$  uncertainties. The measurements, combined assuming Gaussian  
 930 uncertainties, provide 68% and 95% confidence level regions in the  $(\Delta A_{CP}^{\text{dir}}, A_{CP}^{\text{ind}})$  plane,  
 931 denoted with ellipses. The corresponding values for the asymmetries are  $\Delta A_{CP}^{\text{dir}} = (-0.37 \pm$   
 932  $0.45)\%$ ,  $A_{CP}^{\text{ind}} = (-0.35 \pm 2.15)\%$ .

## 934 **XI. SUMMARY**

935 In summary, we report the results of the most sensitive search for  $CP$  violation in singly-  
936 Cabibbo-suppressed  $D^0 \rightarrow \pi^+\pi^-$  and  $D^0 \rightarrow K^+K^-$  decays. We reconstruct signals of  
937  $\mathcal{O}(10^5)$   $D^*$ -tagged decays in an event sample of  $p\bar{p}$  collision data corresponding to approxi-  
938 mately  $5.9 \text{ fb}^{-1}$  of integrated luminosity collected by a trigger on displaced tracks. A fully  
939 data-driven method to cancel instrumental effects provides effective suppression of system-  
940 atic uncertainties to the 0.1% level, approximately half the magnitude of the statistical  
941 uncertainties.

942 We find no evidence of  $CP$  violation and measure  $A_{CP}(D^0 \rightarrow \pi^+\pi^-) = (+0.22 \pm$   
943  $0.24 \text{ (stat)} \pm 0.11 \text{ (syst)})\%$  and  $A_{CP}(D^0 \rightarrow K^+K^-) = (-0.24 \pm 0.22 \text{ (stat)} \pm 0.09 \text{ (syst)})\%$ .  
944 These are the most precise determinations from a single experiment to date, and supersede  
945 the corresponding results of Ref. [16]. The average decay times of the charmed mesons used  
946 in these measurements are  $2.40 \pm 0.03$  units of  $D^0$  lifetime in the  $D^0 \rightarrow \pi^+\pi^-$  sample and  
947  $2.65 \pm 0.03$  units of  $D^0$  lifetime in the  $D^0 \rightarrow K^+K^-$  sample. Assuming negligible  $CP$  viola-  
948 tion in  $D^0 \rightarrow \pi^+\pi^-$  and  $D^0 \rightarrow K^+K^-$  decay widths (direct  $CP$  violation), the above results,  
949 combined with the high-valued average proper decay time of the charmed mesons in our sam-  
950 ple, provide a stringent general constraint on  $CP$  violation in  $D^0$  mixing,  $|A_{CP}^{\text{ind}}(D^0)| < 0.13\%$   
951 at the 90% confidence level. The results probe significant regions of the parameter space  
952 of charm phenomenology where discrimination between SM and non-SM dynamics becomes  
953 possible [30].

## 954 **ACKNOWLEDGMENTS**

955 We thank Y. Grossmann, A. Kagan, A. Petrov, and especially I. I. Bigi and A. Paul for  
956 useful discussions. We thank the Fermilab staff and the technical staffs of the participating  
957 institutions for their vital contributions. This work was supported by the U.S. Department  
958 of Energy and National Science Foundation; the Italian Istituto Nazionale di Fisica Nucleare;  
959 the Ministry of Education, Culture, Sports, Science and Technology of Japan; the Natural  
960 Sciences and Engineering Research Council of Canada; the National Science Council of the  
961 Republic of China; the Swiss National Science Foundation; the A.P. Sloan Foundation; the  
962 Bundesministerium für Bildung und Forschung, Germany; the Korean World Class Uni-

963 versity Program, the National Research Foundation of Korea; the Science and Technology  
 964 Facilities Council and the Royal Society, UK; the Russian Foundation for Basic Research;  
 965 the Ministerio de Ciencia e Innovación, and Programa Consolider-Ingenio 2010, Spain; the  
 966 Slovak R&D Agency; and the Academy of Finland.

967 **Appendix A: Method to suppress detector asymmetries**

968 A mathematical derivation of the concepts described in Sec. V follows. We measure the  
 969  $CP$ -violating asymmetry by determining the asymmetry between number of detected parti-  
 970 cles of opposite charm content  $A = (N_+ - N_-)/(N_+ + N_-)$ , where  $N_+$  and  $N_-$  are the number  
 971 of  $D^0$  and  $\bar{D}^0$  decays found in three different data samples:  $D^*$ -tagged  $D^0 \rightarrow h^+h^-$  decays  
 972 (or simply  $hh^*$ ),  $D^*$ -tagged  $D^0 \rightarrow K^-\pi^+$  decays ( $K\pi^*$ ) and untagged  $D^0 \rightarrow K^-\pi^+$  decays  
 973 ( $K\pi$ ). We show that the combination of asymmetries measured in these three samples yields  
 974 an unbiased estimate of the physical value of  $A_{CP}$  with a high degree of suppression of sys-  
 975 tematic uncertainties coming from detector asymmetries. In the discussion we always refer  
 976 to the *true* values of kinematical variables of particles. The *measured* quantities, affected  
 977 by experimental uncertainties, play no role here since we are only interested in counting  
 978 particles and all detection efficiencies are assumed to be dependent on true quantities only.

979 **1.  $D^*$ -tagged  $D^0 \rightarrow h^+h^-$**

Assuming factorization of efficiencies for reconstructing the neutral charmed meson and the soft pion, we write

$$N_{\pm} = \frac{N^*}{2} B_{D\pi}^* \int dp_* dp_s dp_{h^+} dp_{h^-} \rho_{*\pm}(p_*) B_{hh}^{\pm} \\ \times \rho_{hh^*}(p_{h^+}, p_{h^-}, p_s | p_*) \varepsilon_{hh}(p_{h^+}, p_{h^-}) \varepsilon_{s\pm}(p_s),$$

where  $N^*$  is the total number of  $D^{*+}$  and  $D^{*-}$  mesons;  $p_*$ ,  $p_s$ ,  $p_{h^+}$ ,  $p_{h^-}$  are the three-momenta of the  $D^*$ , soft  $\pi$ ,  $h^+$ , and  $h^-$ , respectively;  $\rho_{*+}$  and  $\rho_{*-}$  are the densities in phase space of  $D^{*+}$  and  $D^{*-}$  mesons (function of the production cross sections and experimental acceptances and efficiencies);  $\rho_{hh^*}$  is the density in phase space of the soft pion and  $h^+h^-$  pair from  $D^0$  decay;  $B_{hh}^+$  and  $B_{hh}^-$  are the branching fractions of  $D^0 \rightarrow h^+h^-$  and  $\bar{D}^0 \rightarrow h^+h^-$ ;  $B_{D\pi}^*$  is the branching fraction of  $D^{*+} \rightarrow D^0\pi^+$  and  $D^{*-} \rightarrow \bar{D}^0\pi^-$ , assumed to be charge-

symmetric;  $\varepsilon_{hh}$  is the detection efficiency of the  $h^+h^-$  pair from the  $D^0$  decay; and  $\varepsilon_{s+}$  and  $\varepsilon_{s-}$  are the detection efficiencies of the positive and negative soft pion, respectively. Conservation of four-momenta is implicitly assumed in all densities. Densities are normalized as  $\int dp_* \rho_{*\pm}(p_*) = 1 = \int dp_s dp_{h^+} dp_{h^-} \rho_{hh^*}(p_{h^+}, p_{h^-}, p_s | p_*)$  for each  $p_*$ . The difference between event yields is therefore

$$\begin{aligned}
N_+ - N_- &= \frac{N_*}{2} B_{D\pi}^* \int dp_* dp_s dp_{h^+} dp_{h^-} \\
&\quad \times \rho_{hh^*}(p_{h^+}, p_{h^-}, p_s | p_*) \varepsilon_{hh}(p_{h^+}, p_{h^-}) \\
&\quad \times \{ \rho_{*+}(p_*) B_{hh}^+ \varepsilon_{s+}(p_s) - \rho_{*-}(p_*) B_{hh}^- \varepsilon_{s-}(p_s) \} \\
&= \frac{N_*}{2} B_{D\pi}^* \int dp_* dp_s dp_{h^+} dp_{h^-} \varepsilon_{hh}(p_{h^+}, p_{h^-}) \\
&\quad \times \rho_{hh^*}(p_{h^+}, p_{h^-}, p_s | p_*) \rho_*(p_*) B_{hh} \varepsilon_s(p_s) \\
&\quad \times [(1 + \delta\rho_*(p_*)) (1 + A_{CP}) (1 + \delta\varepsilon_s(p_s)) \\
&\quad \quad - (1 - \delta\rho_*(p_*)) (1 - A_{CP}) (1 - \delta\varepsilon_s(p_s))],
\end{aligned}$$

where we have defined the following additional quantities:  $\rho_* = (1/2)(\rho_{*+} + \rho_{*-})$ ,  $\delta\rho_* = (\rho_{*+} - \rho_{*-})/(\rho_{*+} + \rho_{*-})$ ,  $B_{hh} = (1/2)(B_{hh}^+ + B_{hh}^-)$ ,  $A_{CP} \equiv A_{CP}(hh) = (B_{hh}^+ - B_{hh}^-)/(B_{hh}^+ + B_{hh}^-)$ ,  $\varepsilon_s = (1/2)(\varepsilon_{s+} + \varepsilon_{s-})$ , and  $\delta\varepsilon_s = (\varepsilon_{s+} - \varepsilon_{s-})/(\varepsilon_{s+} + \varepsilon_{s-})$ . Expanding the products we obtain

$$\begin{aligned}
N_+ - N_- &= N_* B_{D\pi}^* B_{hh} \int dp_* dp_s dp_{h^+} dp_{h^-} \rho_*(p_*) \varepsilon_s(p_s) \\
&\quad \times \rho_{hh^*}(p_{h^+}, p_{h^-}, p_s | p_*) \varepsilon_{hh}(p_{h^+}, p_{h^-}) \\
&\quad \times [A_{CP} + \delta\rho_*(p_*) + \delta\varepsilon_s(p_s) \\
&\quad \quad + A_{CP} \delta\rho_*(p_*) \delta\varepsilon_s(p_s)].
\end{aligned}$$

Since the  $CP$  symmetry of the  $p\bar{p}$  initial state ensures that  $\delta\rho_*(p_*) = -\delta\rho_*(-p_*)$ , the second and fourth term in brackets vanish when integrated over a  $p_*$  domain symmetric in  $\eta$ . In a similar way we obtain

$$\begin{aligned}
N_+ + N_- &= N_* B_{D\pi}^* B_{hh} \int dp_* dp_s dp_{h^+} dp_{h^-} \rho_*(p_*) \varepsilon_s(p_s) \\
&\quad \times \rho_{hh^*}(p_{h^+}, p_{h^-}, p_s | p_*) \varepsilon_{hh}(p_{h^+}, p_{h^-}) \\
&\quad \times [1 + A_{CP} \delta\varepsilon_s(p_s) A_{CP} \delta\rho_*(p_*) \\
&\quad \quad + \delta\varepsilon_s(p_s) \delta\rho_*(p_*)].
\end{aligned}$$

980 The second term in brackets is small with respect to  $A_{CP}$  and can be neglected, while the  
 981 third and fourth terms vanish once integrated over a  $p_*$  domain symmetric in  $\eta$ . Hence the  
 982 observed asymmetry is written as

$$A(hh^*) = \left( \frac{N_+ - N_-}{N_+ + N_-} \right)^{hh^*} = A_{CP}(h^+h^-) + \int dp_s h_s^{hh^*}(p_s) \delta \varepsilon_s(p_s), \text{ where} \quad (\text{A1})$$

$$h_s^{hh^*}(p_s) = \frac{\int dp_* dp_{h^+} dp_{h^-} \rho_*(p_*) \rho_{hh^*}(p_{h^+}, p_{h^-}, p_s | p_*) \varepsilon_{hh}(p_{h^+}, p_{h^-}) \varepsilon_s(p_s)}{\int dp_* dp_{h^+} dp_{h^-} dp_s \rho_*(p_*) \rho_{hh^*}(p_{h^+}, p_{h^-}, p_s | p_*) \varepsilon_{hh}(p_{h^+}, p_{h^-}) \varepsilon_s(p_s)} \quad (\text{A2})$$

983 is the normalized density in phase space of the soft pion for the events included in our  
 984 sample.

## 985 2. $D^*$ -tagged $D^0 \rightarrow K^- \pi^+$

Assuming factorization of efficiencies for reconstructing the neutral charmed meson and the soft pion, we write

$$N_{\pm} = \frac{N^*}{2} B_{D\pi}^* \int dp_* dp_s dp_{\pi} dp_K \rho_{*\pm}(p_*) B_{K\pi}^{\pm} \\ \times \rho_{K\pi^*}(p_K, p_{\pi}, p_s | p_*) \varepsilon_{K\mp\pi\pm}(p_K, p_{\pi}) \varepsilon_{s\pm}(p_s),$$

where  $p_{\pi}$  and  $p_K$  are the three-momenta of the pion and kaon,  $\rho_{K\pi}^*$  is the density in phase space of the soft pion and  $K\pi$  pair from the  $D^0$  decay,  $B_{K\pi}^+$  and  $B_{K\pi}^-$  are the branching fractions of  $D^0 \rightarrow K^- \pi^+$  and  $\bar{D}^0 \rightarrow K^+ \pi^-$ , and  $\varepsilon_{K^- \pi^+}$  and  $\varepsilon_{K^+ \pi^-}$  are the detection efficiencies of the  $K^- \pi^+$  and  $K^+ \pi^-$  pairs from  $D^0$  and  $\bar{D}^0$  decay. The difference between charm and

anti-charm event yields is written as

$$\begin{aligned}
N_+ - N_- &= \frac{N_*}{2} B_{D\pi}^* \int dp_* dp_s dp_\pi dp_K \rho_{K\pi^*}(p_K, p_\pi, p_s | p_*) \\
&\quad \times [\rho_{*+}(p_*) B_{K\pi}^+ \varepsilon_{K-\pi+}(p_K, p_\pi) \varepsilon_{s+}(p_s) \\
&\quad - \rho_{*-}(p_*) B_{K\pi}^- \varepsilon_{K+\pi-}(p_K, p_\pi) \varepsilon_{s-}(p_s)] \\
&= \frac{N_*}{2} B_{D\pi}^* B_{K\pi} \int dp_* dp_s dp_\pi dp_K \rho_*(p_*) \varepsilon_s(p_s) \\
&\quad \times \rho_{K\pi^*}(p_K, p_\pi, p_s | p_*) \varepsilon_{K\pi}(p_K, p_\pi) \\
&\quad \times \{(1 + \delta\rho_*(p_*))(1 + A_{CP}) \\
&\quad \times (1 + \delta\varepsilon_{K\pi}(p_K, p_\pi))(1 + \delta\varepsilon_s(p_s)) \\
&\quad - (1 - \delta\rho_*(p_*))(1 - A_{CP}) \\
&\quad \times (1 - \delta\varepsilon_{K\pi}(p_K, p_\pi))(1 - \delta\varepsilon_s(p_s))\},
\end{aligned}$$

where we have defined the following additional quantities:  $B_{K\pi} = (1/2)(B_{K\pi}^+ + B_{K\pi}^-)$ ,  $A_{CP} \equiv A_{CP}(K\pi) = (B_{K\pi}^+ - B_{K\pi}^-)/(B_{K\pi}^+ + B_{K\pi}^-)$ ,  $\varepsilon_{K\pi} = (1/2)(\varepsilon_{K-\pi+} + \varepsilon_{K+\pi-})$ , and  $\delta\varepsilon_{K\pi} = (\varepsilon_{K-\pi+} - \varepsilon_{K+\pi-})/(\varepsilon_{K-\pi+} + \varepsilon_{K+\pi-})$ . Expanding the products and observing that all terms in  $\delta\rho_*(p_*)$  vanish upon integration over a symmetric  $p_*$  domain, we obtain

$$\begin{aligned}
N_+ - N_- &= N_* B_{D\pi}^* B_{K\pi} \int dp_* dp_s dp_\pi dp_K \rho_*(p_*) \varepsilon_s(p_s) \\
&\quad \times \rho_{K\pi^*}(p_K, p_\pi, p_s | p_*) \varepsilon_{K\pi}(p_K, p_\pi) \\
&\quad \times \{A_{CP} + \delta\varepsilon_{K\pi}(p_K, p_\pi) + \delta\varepsilon_s(p_s) + \dots\},
\end{aligned}$$

where we have neglected one term of order  $A_{CP}\delta^2$ . Similarly,

$$\begin{aligned}
N_+ + N_- &= N_* B_{D\pi}^* B_{K\pi} \int dp_* dp_s dp_\pi dp_K \rho_*(p_*) \varepsilon_s(p_s) \\
&\quad \times \rho_{K\pi^*}(p_K, p_\pi, p_s | p_*) \varepsilon_{K\pi}(p_K, p_\pi) \\
&\quad \times [1 + A_{CP}\delta\varepsilon_{K\pi}(p_K, p_\pi) + A_{CP}\delta\varepsilon_s(p_s) \\
&\quad + \delta\varepsilon_{K\pi}(p_K, p_\pi)\delta\varepsilon_s(p_s)].
\end{aligned}$$

<sup>986</sup> If we neglect all terms of order  $A_{CP}\delta$  and  $\delta^2$ , we finally obtain

$$A(K\pi^*) = \left( \frac{N_+ - N_-}{N_+ + N_-} \right)^{K\pi^*} = A_{CP}(K^-\pi^+) + \int dp_\pi h_{K\pi}^{K\pi^*}(p_K, p_\pi) \delta\varepsilon_{K\pi}(p_K, p_\pi) + \int dp_s h_s^{K\pi^*}(p_s) \delta\varepsilon_s(p_s), \quad (\text{A3})$$

$$\text{where } h_{K\pi}^{K\pi^*}(p_K, p_\pi) = \frac{\int dp_* dp_s \rho_*(p_*) \rho_{K\pi^*}(p_K, p_\pi, p_s | p_*) \varepsilon_{K\pi}(p_K, p_\pi) \varepsilon_s(p_s)}{\int dp_* dp_\pi dp_K dp_s \rho_*(p_*) \rho_{K\pi^*}(p_K, p_\pi, p_s | p_*) \varepsilon_{K\pi}(p_K, p_\pi) \varepsilon_s(p_s)}, \quad (\text{A4})$$

987 and  $h_s^{K\pi^*}(p_s)$  (the  $K\pi$  analogous to  $h_s^{hh^*}(p_s)$  in Eq. A2) are the normalized densities in phase  
988 space of  $\pi, K$  and soft  $\pi$ , respectively, for the events included in our sample.

### 989 3. Untagged $D^0 \rightarrow K^-\pi^+$

In this case

$$\begin{aligned} N_\pm &= \frac{N_0}{2} \int dp_0 dp_\pi dp_K \rho_{0\pm}(p_0) B_{K\pi}^\pm \\ &\quad \times \rho_{K\pi}^0(p_K, p_\pi | p_0) \varepsilon_{K\mp\pi\pm}(p_K, p_\pi) \\ N_+ - N_- &= \frac{N_0}{2} B_{K\pi} \int dp_0 dp_\pi dp_K \\ &\quad \times \rho_0(p_0) \rho_{K\pi}^0(p_K, p_\pi | p_0) \varepsilon_{K\pi}(p_K, p_\pi) \\ &\quad \times \{(1 + \delta\rho_0(p_0))(1 + A_{CP})(1 + \delta\varepsilon_{K\pi}(p_K, p_\pi)) \\ &\quad - (1 - \delta\rho_0(p_0))(1 - A_{CP})(1 - \delta\varepsilon_{K\pi}(p_K, p_\pi))\} \end{aligned}$$

where we have defined the following quantities  $\rho_0 = (1/2)(\rho_{0+} + \rho_{0-})$  and  $\delta\rho_0 = (\rho_{0+} - \rho_{0-})/(\rho_{0+} + \rho_{0-})$ . Assuming  $\eta$  symmetry of the  $p_0$  integration region,

$$\begin{aligned} N_+ - N_- &= N_0 B_{K\pi} \int dp_0 dp_\pi dp_K \rho_0(p_0) \rho_{K\pi}^0(p_K, p_\pi | p_0) \\ &\quad \times \varepsilon_{K\pi}(p_K, p_\pi) [A_{CP} - \delta\varepsilon_{K\pi}(p_K, p_\pi)]. \end{aligned}$$

Similarly we obtain

$$\begin{aligned} N_+ + N_- &= N_0 B_{K\pi} \int dp_0 dp_\pi dp_K \rho_0(p_0) \rho_{K\pi}^0(p_K, p_\pi | p_0) \\ &\quad \times \varepsilon_{K\pi}(p_K, p_\pi) [1 + A_{CP} \delta\varepsilon_{K\pi}(p_K, p_\pi)], \end{aligned}$$

990 and neglecting the second term in brackets,

$$\begin{aligned}
A(K\pi) &= \left( \frac{N_+ - N_-}{N_+ + N_-} \right)^{K\pi} = A_{CP}(K^- \pi^+) + \int dp_\pi dp_K h_{K\pi}^{K\pi}(p_K, p_\pi) \delta\varepsilon_{K\pi}(p_K, p_\pi), \text{ where} \\
h_{K\pi}^{K\pi}(p_K, p_\pi) &= \frac{\int dp_0 \rho_0(p_0) \rho_{K\pi}^0(p_K, p_\pi | p_0) \varepsilon_{K\pi}(p_K, p_\pi)}{\int dp_0 dp_\pi dp_K \rho_0(p_0) \rho_{K\pi}^0(p_K, p_\pi | p_0) \varepsilon_{K\pi}(p_K, p_\pi)} \quad (\text{A5})
\end{aligned}$$

991 is the normalized density in phase space of the  $K\pi$  system in the events included in our  
992 sample.

#### 993 4. Combining the asymmetries

994 By combining the asymmetries measured in the three event samples we obtain

$$\begin{aligned}
A(hh^*) - A(K\pi^*) + A(K\pi) &= A_{CP}(h^+ h^-) + \int dp_s h_s^{hh^*}(p_s) \delta\varepsilon_s(p_s) \\
&\quad - A_{CP}(K^- \pi^+) - \int dp_K dp_\pi h_{K\pi}^{K\pi^*}(p_K, p_\pi) \delta\varepsilon_{K\pi}(p_K, p_\pi) - \int dp_s h_s^{K\pi^*}(p_s) \delta\varepsilon_s(p_s) \\
&\quad + A_{CP}(K^- \pi^+) + \int dp_K dp_\pi h_{K\pi}^{K\pi}(p_K, p_\pi) \delta\varepsilon_{K\pi}(p_K, p_\pi) = A_{CP}(h^+ h^-), \quad (\text{A6})
\end{aligned}$$

995 where we assumed  $h_s^{K\pi^*}(p_s) = h_s^{hh^*}(p_s)$ , and  $h_{K\pi}^{K\pi^*}(p_K, p_\pi) = h_{K\pi}^{K\pi}(p_K, p_\pi)$ . The last two  
996 equalities are enforced by appropriate kinematic reweighing of the event samples. We need to  
997 equalize distributions with respect to the true momenta while we only access the distributions  
998 with respect to the measured momenta. Hence the assumption that event samples that have  
999 the same distribution with respect to the measured quantities also have the same distribution  
1000 with respect to the true quantities is needed.

1001 The mathematical derivation shows that for small enough physics and detector-induced  
1002 asymmetries, the linear combination of the observed asymmetries used in this measure-  
1003 ment achieves an accurate cancellation of the instrumental effects with minimal impact on  
1004 systematic uncertainties.

#### 1005 Appendix B: Monte Carlo test of the analysis technique

1006 We tested the suppression of instrumental effects by repeating the analysis in simulated  
1007 samples in which known instrumental and physics asymmetries were introduced. Many  
1008 different configurations for the input asymmetries were tested, covering a rather extended

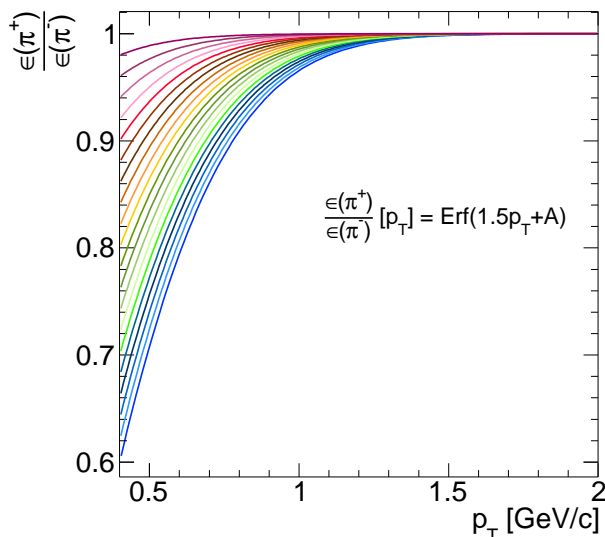


FIG. 18. Curves corresponding to simulated ratios of efficiencies for reconstructing positive versus negative pions as a function of transverse momentum.

1009 range, to ensure the reliability of the method independently of their actual size in our data.  
 1010 For each configuration,  $\mathcal{O}(10^6)$  decays were simulated to reach the desired 0.1% sensitivity.  
 1011 Only the  $D^0 \rightarrow \pi^+\pi^-$  sample was tested although the results are valid for the  $D^0 \rightarrow K^+K^-$   
 1012 case as well.

1013 We test cancellation of instrumental effects arising from different reconstruction efficien-  
 1014 cies between positive and negative particles, which in general depend on the particle species  
 1015 and momentum. Furthermore, the reliability of the suppression should not depend on the  
 1016 actual size of  $CP$  violation in  $D^0 \rightarrow K^-\pi^+$  and  $D^0 \rightarrow \pi^+\pi^-$  decays.

1017 We repeated the measurement on statistical ensembles where the above effects are known  
 1018 and arbitrarily varied using a combination of event-specific weights applied to the true values  
 1019 of simulated quantities. Each ensemble consists of approximately one thousand trials. We  
 1020 compare the resulting observed asymmetry  $A_{CP}^{\text{obs}}(\pi\pi)$  to the one given in input,  $A_{CP}^{\text{true}}(\pi^+\pi^-)$ ,  
 1021 by inspecting the distribution of the residual,  $\Delta A_{CP}(\pi\pi) = A_{CP}^{\text{obs}}(\pi^+\pi^-) - A_{CP}^{\text{true}}(\pi^+\pi^-)$ .

1022 We first investigate the individual impact of each effect. We scan the value of a single  
 1023 input parameter across a range that covers larger variations than expected in data and as-  
 1024 sume all other effects are zero. First a  $p_T$ -dependent function that represents the dependence  
 1025 observed in data (see Fig. 1) is used to parameterize the soft pion reconstruction efficiency

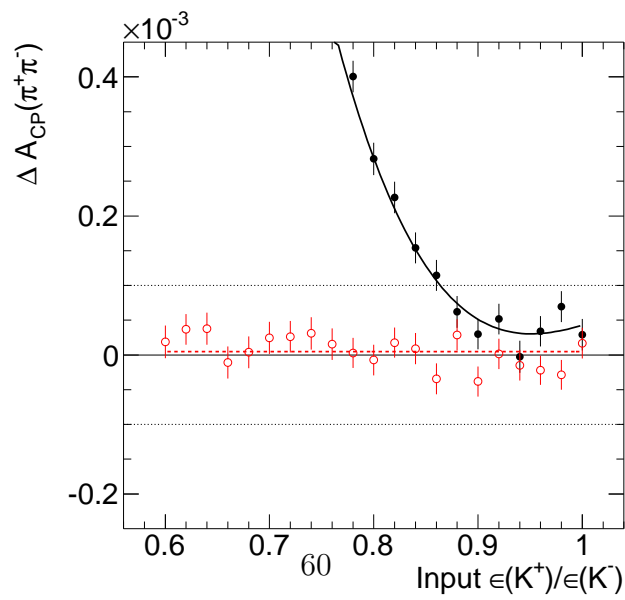
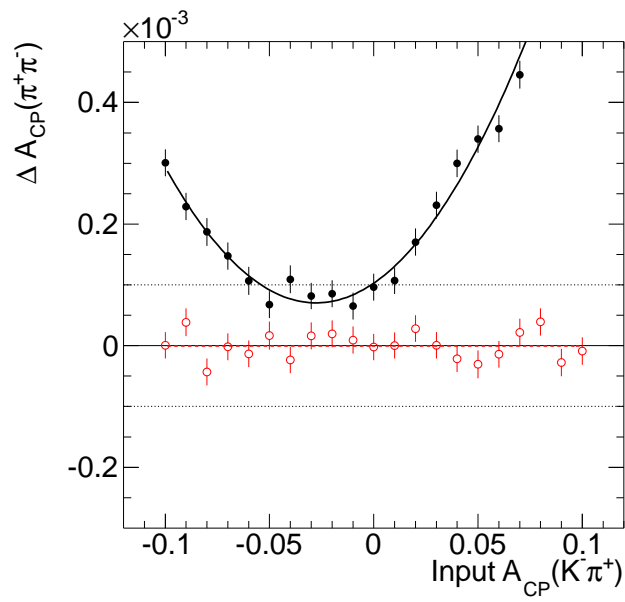
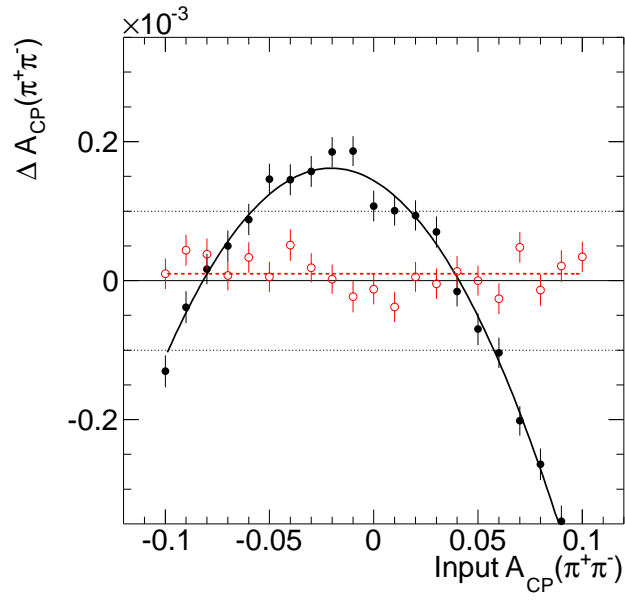
1026 ratio as  $\epsilon(\pi^+)/\epsilon(\pi^-) = \text{Erf}(1.5 \cdot p_T + A)$ , where  $p_T$  is in GeV/ $c$  and various values of the  
 1027 constant  $A$  have been tested so that the efficiency ratio at 0.4 GeV/ $c$  spans the 0.6–1 GeV/ $c$   
 1028 range as shown in Fig. 18. Then, the kaon reconstruction efficiency ratio  $\epsilon(K^-)/\epsilon(K^+)$  is  
 1029 varied similarly in the 0.6–1 GeV/ $c$  range. Finally, a range  $-10\% < A_{CP} < 10\%$  is tested  
 1030 for the physical  $CP$ -violating asymmetry in  $D^0 \rightarrow K^-\pi^+$  and  $D^0 \rightarrow \pi^+\pi^-$  decays.

1031 The results are shown in Fig. 19 (empty dots). The cancellation of instrumental asym-  
 1032 metries is realized at the sub-per mil level even with input effects of size much larger than  
 1033 expected in data.

1034 Figure 19 (filled dots) shows the results of a more complete test in which other ef-  
 1035 fects are simulated, in addition to the quantities varied in the single input parameter  
 1036 scan: a  $p_T$ -dependent relative efficiency  $\epsilon(\pi^+)/\epsilon(\pi^-)$ , corresponding to 0.8 at 0.4 GeV/ $c$ ,  
 1037  $\epsilon(K^-)/\epsilon(K^+) = 98\%$ ,  $A_{CP}(K\pi) = 0.8\%$  and  $A_{CP}(\pi\pi) = 1.1\%$ . Larger variations of the  
 1038 residual are observed with respect to the previous case. This is expected because mixed  
 1039 higher-order terms corresponding to the product of different effects are not canceled and  
 1040 become relevant.

1041 Finally we tested one case with more realistic values for the input effects. The  $p_T$  depen-  
 1042 dence of  $\epsilon(\pi^+)/\epsilon(\pi^-)$  is extracted from fitting data (Fig. 1) to be distributed as  $\text{Erf}(2.49 p_T)$ ,  
 1043 with  $p_T$  in GeV/ $c$ . We used  $\epsilon(K^+)/\epsilon(K^-) \approx \epsilon(K^+\pi^-)/\epsilon(K^-\pi^+) = 1.0166$ , in which the ap-  
 1044 proximation holds assuming equal efficiency for reconstructing positive and negative pions  
 1045 at  $p_T > 2$  GeV/ $c$  [31]. We assume  $A_{CP}(K\pi) = 0.1\%$ , ten times larger than the current  
 1046 experimental sensitivity. A  $-5\% < A_{CP}(\pi\pi) < 5\%$  range is tested in steps of 0.5% for  
 1047 the physical asymmetry to be measured. The results are shown in Fig. 20. The maximum  
 1048 observed bias is of the order of 0.02%, one order of magnitude smaller than the statistical  
 1049 resolution on the present measurement. The observed bias is  $(0.0077 \pm 0.0008)\%$  averaged  
 1050 over the  $A_{CP}(\pi\pi)$  range probed. These results, which extend to the  $K^+K^-$  case, demon-  
 1051 strate the reliability of our method in extracting a precise and unbiased measurement of  $CP$   
 1052 violation in  $D^0$  meson decays into  $K^+K^-$  and  $\pi^+\pi^-$  final states, even in the presence of  
 1053 sizable instrumental asymmetries.

1054 The results discussed in this appendix are used in Sec. IX to estimate a systematic  
 1055 uncertainty on the final results due to neglecting higher order terms in Eq. (6), including



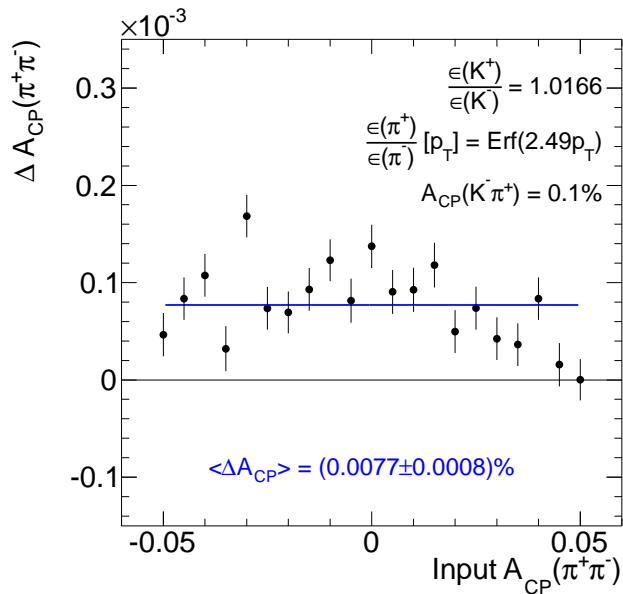


FIG. 20. Asymmetry residual as a function of the physical  $CP$ -violating asymmetry in  $D^0 \rightarrow \pi^+\pi^-$  decays. Realistic effects other than shown in the scan are also simulated. The line represents the value averaged over the  $-5\% < A_{CP}(\pi\pi) < 5\%$  range.

1056 possible non-factorization of  $h^+h'^-$  and  $\pi_s$  reconstruction efficiencies.

- 
- 1057 [1] K. Nakamura *et al.* (Particle Data Group), J. Phys. G **37**, 075021 (2010) and 2011 partial  
1058 update for the 2012 edition.
- 1059 [2] S. Bianco, F. L. Fabbri, D. Benson, and I. I. Bigi, Riv. Nuovo Cim. **26N7**, 1 (2003).
- 1060 [3] D. Asner *et al.*, arXiv:1010.1589 and online update at  
1061 <http://www.slac.stanford.edu/xorg/hfag>.
- 1062 [4] M. Artuso, B. Meadows, and A. A. Petrov, Ann. Rev. Nucl. Part. Sci. **58**, 249 (2008).
- 1063 [5] I. Shipsey, Int. J. Mod. Phys. A **21**, 5381 (2006).
- 1064 [6] G. Burdman and I. Shipsey, Ann. Rev. Nucl. Part. Sci. **53**, 431 (2003).
- 1065 [7] Y. Nir and N. Seiberg, Phys. Lett. B **309**, 337 (1993).
- 1066 [8] M. Ciuchini *et al.*, Phys. Lett. B **655**, 162 (2007).
- 1067 [9] B. Aubert *et al.* (BABAR Collaboration), Phys. Rev. Lett. **98**, 211802 (2007).
- 1068 [10] M. Staric *et al.* (Belle Collaboration), Phys. Rev. Lett. **98**, 211803 (2007).

- 1069 [11] T. Aaltonen *et al.* (CDF Collaboration), Phys. Rev. Lett. **100**, 121802 (2008).
- 1070 [12] A. A. Petrov, Int. J. Mod. Phys. A **21**, 5686 (2006).
- 1071 [13] E. Golowich, J. Hewett, S. Pakvasa, and A. A. Petrov, Phys. Rev. D **76**, 095009 (2007).
- 1072 [14] B. Aubert *et al.* (*BABAR* Collaboration), Phys. Rev. Lett. **100**, 061803 (2008).
- 1073 [15] M. Staric *et al.* (Belle Collaboration), Phys. Lett. B **670**, 190 (2008).
- 1074 [16] D. E. Acosta *et al.* (CDF Collaboration), Phys. Rev. Lett. **94**, 122001 (2005).
- 1075 [17] L. Balka *et al.*, Nucl. Instrum. Methods A **267**, 272 (1988); S. Bertolucci *et al.*, Nucl. Instrum.  
1076 Methods A **267**, 301 (1988); M. Albrow *et al.*, Nucl. Instrum. Methods A **480**, 524 (2002);  
1077 and G. Apollinari *et al.*, Nucl. Instrum. Methods A **412**, 515 (1998).
- 1078 [18] G. Ascoli *et al.*, Nucl. Instrum. Methods A **268**, 33 (1988).
- 1079 [19] T. Affolder *et al.*, Nucl. Instrum. Methods A **526**, 249 (2004).
- 1080 [20] A. Sill *et al.*, Nucl. Instrum. Methods A **447**, 1 (2000).
- 1081 [21] C. S. Hill *et al.*, Nucl. Instrum. Meth. A **530**, 1 (2004).
- 1082 [22] A. Affolder *et al.*, Nucl. Instrum. Meth. A **453**, 84 (2000).
- 1083 [23] E. J. Thomson *et al.*, IEEE Trans. Nucl. Sci. **49**, 1063 (2002); R. Downing *et al.*, Nucl.  
1084 Instrum. Methods, A **570**, 36 (2007).
- 1085 [24] L. Ristori and G. Punzi, Annu. Rev. Nucl. Part. Sci. **60**, 595 (2010); W. Ashmanskas *et al.*,  
1086 Nucl. Instrum. Methods, A **518**, 532 (2004).
- 1087 [25] A. Di Canto, Ph.D. Thesis, University of Pisa, Fermilab Report No. FERMILAB-THESIS-  
1088 2011-29 (2011).
- 1089 [26] N. L. Johnson, Biometrika **36**, 149 (1949).
- 1090 [27] S. Bar-Shalom, G. Eilam, M. Gronau, and J. L. Rosner, Phys. Lett. B **694**, 374 (2011).
- 1091 [28] M. Golden and B. Grinstein, Phys. Lett. B **222**, 501 (1989).
- 1092 [29] F. Buccella *et al.*, Phys. Rev. D **51**, 3478 (1995).
- 1093 [30] I. I. Bigi, A. Paul, and S. Recksiegel, J. High Energy Phys. 06 (2011) 089.
- 1094 [31] T. Aaltonen *et al.* (CDF Collaboration), Phys. Rev. Lett. **106**, 181802 (2011).